Unusually heavy stable Mo isotope signatures of the Ottawa River: causes and implications for global riverine Mo fluxes

O'Sullivan, E.M.[1]*, Nägler, T.F. [1] and Babechuk, M.G.[2]

[1]Institute of Geological Sciences, University of Bern, Bern, Switzerland

[2]Department of Earth Sciences, Memorial University of Newfoundland, St. John's, Canada

*Correspondence: edel.osullivan@geo.unibe.ch

Keywords: molybdenum isotopes; rivers; Ottawa River; SLRS-6; surface cycle; anthropogenic

Abstract

The accurate use of Mo isotope mass balance modelling of ancient oceans relies on the assumption that the δ^{98}Mo of modern riverine inputs represents a reasonable estimate of the past. A growing number of studies of global rivers have demonstrated significant variation in δ^{98}Mo from the bedrock sources of Mo. The Ottawa River, Canada, was previously identified as having an anomalously heavy Mo isotope composition, with a δ^{98}Mo signature close to seawater (2.3‰), for a seemingly pristine natural river. To further explore this unusual signature, we collected and filtered 29 water samples from the Ottawa River, tributaries, and small lakes, and analysed them for Mo isotopes as well as major and trace elements. Here, we fully document heavy δ^{98}Mo signatures throughout the Ottawa River and its absence in surrounding areas of the wider Ottawa River basin (ORB). Our results reveal a progressive upstream increase in both Mo concentration and δ^{98}Mo signatures in the Ottawa River towards values even heavier than seawater, up to 3.13‰ – the heaviest Mo isotopic signature of river water measured to date. In contrast, the tributaries and lakes display far lighter and more consistent δ^{98}Mo signatures within the range previously found in other rivers. Weathering of an isotopically heavy bedrock source, fractionation during weathering and retention of light isotopes in soils have all been proposed as sources of heavy δ^{98}Mo in rivers; however, none of these mechanisms can satisfactorily explain our new observations. Colloidal and particulate processes that remove elements downstream, as inferred from some trace element proxies, also cannot explain the decreasing δ^{98}Mo, since the preferential removal of

light Mo isotopes is predicted from these processes. Similarly, the downstream trends show no apparent relationships with constructed dams or known potential industrial sources. Therefore, our findings from the Ottawa River are best explained as the dilution of a yet unidentified point source of heavy Mo upstream of sampling, or a significant permanent sink for light isotopes existing only in the upper reaches of the catchment. In both cases, anthropogenic contribution from a large mining district in the headwaters of the river must be considered and should be explored further. Fractionation of Mo in waste rock storage facilities have been previously identified and may provide an unnatural sink for isotopically light Mo through the Rayleigh-type fractionation of dissolved Mo on oxyhydr(oxide) mineral surfaces. The implied anthropogenic alteration of the natural Mo cycle highlights the significant and wide-reaching effects of unnatural point sources of Mo on the cumulative δ^{98}Mo signatures of the catchment, and emphasises the necessity for detailed geochemical screening of anomalous river water isotope signatures before natural isotope compositions are inferred.

1. Introduction

In recent decades, the importance of molybdenum (Mo) as a bioessential nutrient and its efficacy as a redox tracer has propelled the refinement of our understanding of the modern Mo surface cycle (e.g. Barling *et al.,* 2001; Kendall *et al.,* 2017; Miller *et al.,* 2011; Scott *et al.,* 2008; Siebert *et al.,* 2003). Molybdenum is the most abundant and homogenously distributed transition metal in the modern ocean (Collier, 1985) at ~0.11μM, where it is present mainly as the highly soluble molybdate oxyanion MoO_4^{2-} (Erickson and Helz, 2000). The highly conservative nature of this species in oxic waters results in a long residence time of between ~450Ka (Miller *et al.,* 2011) and ~800Ka (Collier, 1985; Lutfi Firdaus *et al.,* 2008). Oceanic molybdate is sourced primarily from the oxic weathering of Mo-rich minerals in the continental crust (Arnórsson and Óskarsson, 2007; Greaney *et al.,* 2018) and delivered via riverine runoff (McManus *et al.,* 2002; McManus *et al.,* 2006; Morford and Emerson, 1999), with a less significant source from hydrothermal fluids (1-13% that of the riverine flux, Wheat *et al.,* 2002). Removal of Mo from ocean water either by co-precipitation with ferromanganese oxides or by variable scavenging by organic matter in suboxic to anoxic or weakly euxinic environments produces significant fractionation effects favouring the light isotopes (Barling and Anbar, 2004; Barling *et al.,* 2001; Neubert *et al.,* 2008; Siebert *et al.,* 2003; Scott and Lyons, 2012), contributing to a homogenous heavy δ^{98}Mo signature of ocean water of +2.3‰ (Siebert *et al.,* 2003; Nakagawa *et al.,* 2012; relative to NIST SRM 3134 = +0.25‰, following Nägler *et al.,* 2014). In strongly euxinic environments, thiomolybdate ions are quasi-quantitatively scavenged, resulting in minimal net fractionation of Mo isotopes (Erickson and Helz, 2000; Helz *et al.,* 1996; Nägler *et al.,* 2005, Neubert *et al.,* 2008).

Sedimentary rocks recording Mo sinks in each of the aforementioned redox environments (e.g. black shale, iron formation) are routinely used as archives of past ocean isotope composition and are

studied with the aim of reconstructing the timing and nature of ocean-atmosphere oxygenation (Arnold *et al.,* 2004; Baldwin *et al.,* 2013; Kurzweil *et al.,* 2015a; Kurzweil *et al.,* 2015b; Siebert *et al.,* 2003; Voegelin *et al.,* 2010; Wille *et al.,* 2007). However, in order to extract global-scale inferences of ocean-atmosphere oxygenation, a box-model approach is required (Arnold *et al.,* 2004; Cheng *et al.,* 2015; Lehmann *et al.,* 2007; Lu *et al.,* 2017; McManus *et al.,* 2006; Pearce *et al.,* 2008; Siebert *et al.,* 2003; Wille *et al.,* 2008). A record of the Mo isotope composition of contemporaneous seawater can be obtained from black shale and other marine archives (Baldwin *et al.,* 2013; Erickson and Helz, 2000; Helz *et al.,* 1996; Kurzweil *et al.,* 2015a; Kurzweil *et al.,* 2015b; Nägler *et al.,* 2005; Nägler *et al.,* 2011; Thoby *et al.,* 2019; Voegelin *et al.,* 2009; Voegelin *et al.,* 2010; Wen *et al.,* 2011; Wille *et al.,* 2007; Xu *et al.,* 2012; Zhou *et al.,* 2015), but models require an assumption of the isotope composition of Mo inputs into the ocean. The assumed δ^{98}Mo of inputs in early mass balance models was ~0‰, close to that of molybdenites and crustal igneous rocks (e.g. Barling *et al.,* 2001; Siebert *et al.,* 2003). However, this value was later assumed to be slightly heavier at ~+0.7 - +0.8‰ based on average values calculated from major rivers across the globe that are inferred to be influenced only by naturally occurring process, i.e., free of major anthropogenic disturbance (Archer and Vance, 2008).

The average global riverine Mo isotope signature has become progressively better characterised throughout the last decade (Archer and Vance, 2008; Horan *et al.,* 2020; King and Pett-Ridge, 2018; Neely *et al.,* 2018; Neubert *et al.,* 2011; Pearce *et al.,* 2010; Voegelin *et al.,* 2012). At present, perhaps the most comprehensive compilation of published river water δ^{98}Mo and annual Mo discharge data is provided by King and Pett-Ridge (2018). The weighted average of this compiled data gives an estimate of the global continental δ^{98}Mo signature of +0.8‰ (excluding groundwater data), which is similar to previous estimates (e.g. +0.7‰ proposed by Archer and Vance, 2008). These compilations and estimates include the anomalously heavy δ^{98}Mo composition (~+2.3‰) of the Ottawa River, Canada, derived from the certified reference material SLRS-4 analysed by Archer and Vance (2008). This δ^{98}Mo value for the Ottawa River was assumed by Archer and Vance (2008) to be a "pristine" record of natural processes, such as removal of isotopically light Mo on soil particle surfaces, due to the large size of the Ottawa River basin (ORB) relative to its minimal anthropogenic footprint. However, even after a subsequent decade of additional Mo isotope work on rivers, the Ottawa River value remains isotopically heavier than any other river water analysed to date. Since the publication of the SLRS-4 values by Archer and Vance (2008), there have been no follow-up reports on the Mo isotope composition of SLRS-5 and SLRS-6, the two subsequent generations of the SLRS CRM from the Ottawa River. Accordingly, there are no constraints on how repeatable and widespread the unusual Mo isotope composition is within the ORB.

The objective of this study is to revisit the unusually heavy Mo isotope composition in the dissolved load of the Ottawa River to better constrain the origin of heavy Mo isotope enrichment. This study reports new δ^{98}Mo values from SLRS-6 as well as 29 new samples of a ~300km transect of the

Ottawa River between Temiscaming and Chenaux and selected tributaries and ponds/lakes. The results offer new insights into ORB Mo isotope geochemistry that explore the relative roles of natural catchment-scale processes and various potential direct or indirect anthropogenic sources (e.g. damming of river water, inputs from localized industries, and point sources related to base metal mining in northern areas of the ORB). This study has important implications for the assessment of riverine δ^{98}Mo compositions within large river catchments and the effect that cryptic anthropogenic influences may have on estimates of global riverine Mo input signatures.

1.1 Mo cycling and isotope fractionation in continental environments

Relative to most igneous crustal rocks with a comparatively limited range of bulk δ^{98}Mo from ~-0.5 - +0.8‰ (Greber *et al.,* 2014; Greber *et al.,* 2015; Horan *et al.,* 2020; Liu *et al.,* 2020; Pearce *et al.,* 2010; Siebert *et al.,* 2003; Voegelin *et al.,* 2014; Willbold *et al.,* 2016; Zhao *et al.,* 2016), rivers from across the globe have highly variable and generally heavy δ^{98}Mo signatures from ~-0.2 to +2.3‰ (Archer and Vance, 2008; King and Pett-Ridge, 2018; Neely *et al.,* 2018; Neubert *et al.,* 2011; Pearce *et al.,* 2010; Rahaman *et al.,* 2014; Voegelin *et al.,* 2012; Wang *et al.,* 2015). The primary driver of the variability in riverine Mo isotope composition has been the subject of a largely two-sided debate between Mo source and Mo sink controls.

Those in favour of a Mo source-origin argue that the composition of many rivers reflect that of the underlying bedrock from which the Mo is derived, including isotopically heavy sedimentary rocks such as marine evaporates and black shales (Neely *et al.,* 2018; Neubert *et al.,* 2011; Pearce *et al.,* 2010; Lehmann *et al.,* 2007; Wang *et al.,* 2015). Experimental leaching of bulk granites and sulfides indicate minimal fractionation directly associated with the mobilisation and release of Mo from the host material (Siebert *et al.,* 2003; Skierszkan *et al.,* 2016), whereas incongruent leaching of Mo-rich, isotopically heavy components of igneous rocks relative to bulk composition leads to the enrichment of the fluids to the same extent of the leachates (Voegelin *et al.,* 2012).

Conversely, those in favour of a Mo sink-origin argue for the preferential retention of light isotopes in the weathering profile and soils during oxic weathering (Archer and Vance, 2008; Horan *et al.,* 2020; Kashiwabara *et al.*, 2011; Liermann *et al.,* 2011; Wang *et al.,* 2018; Wang *et al.,* 2020). Adsorption of mobilised molybdate to Fe-, Mn-, Ti- and Al- (oxyhydr)oxides and clay minerals has been shown to occur through inner sphere complexation of MoO_4^{2-} via ligand exchange with surface hydroxyl ions and is highly pH dependent, with maximum adsorption occurring at pH 4, decreasing with increasing pH (Goldberg *et al.,* 1996; Kashiwabara *et al.*, 2011). Though the precise mechanism of fractionation upon adsorption has so far not been confirmed, possible mechanisms favouring the light isotopes include kinetic affects during complexation, differing bond strengths and coordination changes (e.g. Goldberg *et al.,* 2009; Malinovsky *et al.,* 2007). Secondary minerals such as Fe(oxyhydr)oxides and organic matter in soils and weathering profiles have been repeatedly (though not universally) found to host isotopically light Mo relative to the unweathered bedrock (Goldberg *et al.,* 2009; Horan *et al.,*

2020; King *et al.,* 2018; King *et al.,* 2016; Marks *et al.,* 2015; Wang *et al.,* 2015; Wang *et al.,* 2018; Wang *et al.,* 2020), supporting the notion that the release of isotopically heavy residual porewaters into rivers following Mo adsorption exerts a significant control on the river water δ^{98}Mo signatures.

Although retention of Mo appears to generally favour light isotopes in comparison to typical crustal values (global bulk soil δ^{98}Mo data ranging from ~-1.5 to +0.5‰, Horan *et al.*, 2020; Wang *et al.*, 2020), a simple relationship between soil and river water Mo isotope data via soil processes is not always apparent. For example, a riverine δ^{98}Mo controlled primarily by secondary oxide minerals in weathering profiles is at odds with Amazon basin river data with δ^{98}Mo signatures close to crustal compositions (+0.57 - +0.63‰; Archer and Vance, 2008), despite the deeply weathered underlying lateritic soils. The re-release of adsorbed Mo within soils by downward leaching of light Mo in shallow soils and subsequent re-adsorption within deeper horizons has also been observed (Wang *et al.,* 2018), bringing to question the irreversibility of Mo retention within soils as they should eventually reach steady state over geological timescales (Neubert *et al.,* 2011; Zeng *et al.,* 2019). The effect of changing soil pH (e.g. during seasonal changes in precipitation, Slessarev *et al.,* 2016), redox conditions (Siebert *et al.,* 2015; Wang *et al.,* 2020), and seasonal fluctuations in oxide formation in soils (Rondeau *et al.,* 2005; and references therein) are so far not confirmed. In summary, it is not always clear or traceable at a catchment scale that soils form a stable and steady state reservoir of light Mo isotopes, especially since few studies measure different reservoirs in parallel. Further, the relative importance of precipitation and biological cycling has been a topic of some studies, though so far their effect on the isotope composition in soils and stream water is inconclusive (e.g. Marks *et al.,* 2015; Nägler *et al.,* 2020; Wang *et al.,* 2020).

An additional factor that is emerging as a potential influence on the Mo surface cycle is that of anthropogenic Mo input (King *et al.,* 2016; Neubert *et al.,* 2011), most notably in settings adjacent to human activities such as smelters and mine waste rock storage facilities, providing point sources of anthropogenically altered Mo to rivers with potentially far-reaching effects (Chappaz *et al.,* 2008; Chappaz *et al.,* 2012; Skierszkan *et al.,* 2016; Skierszkan *et al.,* 2017; Skierszkan *et al.,* 2019). Most significant to the study of factors contributing to heavy isotope signatures in river basins is the observation of Mo isotope fractionation associated with acid mine drainage emitted from waste rock storage facilities within molybdenite mines (Skierszkan *et al.,* 2016; Skierszkan *et al.,* 2017; Skierszkan *et al.,* 2019). Although these studies have so far focused on isotope fractionation specific to flow paths within the mining settings, it provides a basis for the study of the transfer of these anthropogenic dissolved Mo signatures enriched in heavy Mo isotopes in waters throughout the wider scale of a hydrological catchment.

2. Background and sampling locations

2.1 The Ottawa River

2.1.1 Drainage Basin, hydrology and bedrock geology

A major tributary of the St. Lawrence River basin, the Ottawa River originates in Lac des Outaouais and Lac Capimitchigama, Quebec, approximately 240 km North of Ottawa City, where it flows westwards through a series of complex lake systems until it drains into Lake Timiskaming. Here the river turns south towards Mattawa and then eastwards through the cities of Ottawa and Montreál, where it enters the St. Lawrence River that ultimately flows north-eastwards into the Atlantic Ocean (Figure 1). The river is over 1,271 km long and drains an area of 146,334 km^2 (Ventura *et al.,* 2005), with a mean annual discharge of 1,965 $m^3 s^{-1}$ (average of annual means at Carillon from January 1964 to March 2019, Ottawa River Regulation Planning Board, 2011; retrieved 05.11.2019). The Ottawa River contributes approximately 0.2% of the total global riverine freshwater discharge to the oceans (calculated using estimated global riverine discharge from Dai and Trenberth, 2002). Peak discharge occurs from March-May with an annual low discharge during July and August. Peak discharge in 2018 occurred in the month of May with an average discharge of 4,467 $m^3 s^{-1}$, with the lowest average discharge of 1,104 $m^3 s^{-1}$ occurring in August. Numerous tributaries and streams flow into the Ottawa River, the largest of which are the Montreal, Noire, Petawawa and Coulonge Rivers, each over 200 km in length, and the shorter Mattawa River that drains from Lake Trout in the west.

Soil cover in the ORB is relatively thin, apart from a large glaciolacustrine clay belt stretching from the Cochrane District, Ontario to Abitibi County, Quebec. Upper basin soil cover consists of a mixture of well drained organic mesisols and podzols with silt and sand deposits from the Champlain Sea, whereas in lower sections consist of well-drained podzols with some poorly-drained melanic brunisols near the confluence with the St. Lawrence River (Thorp *et al.,* 2005). The river is in the Temperate Deciduous and Boreal Forest biomes, and marshes and swamps are a common occurrence in the floodlands surrounding the river. Flooding is frequent during the seasonal release of meltwater from March to May (Thorp *et al.,* 2005). Soils of the region of Quebec and Southeast Ontario are generally mildly to moderately acidic (IGBP-DIS Global Soils Dataset, 1998)

The underlying bedrock of the ORB is silicate-dominated in the central to northern areas and more carbonate and siliciclastic sedimentary rock-dominated in the southern areas (Figure 1). Overall, the Ottawa River and many of its tributaries originate in felsic Archean-Proterozoic granitoids or metamorphosed equivalents and only flow over younger Phanerozoic bedrock and/or Quaternary sediments in the southern ORB. More specifically, metamorphosed mafic to felsic volcanic rocks of the Abitibi greenstone belt and Proterozoic low-grade metamorphic sedimentary rocks of the Huronian

Supergroup dominate the north to northwest of the catchment where the headwaters of the Ottawa River originate. In its entirety, the Archaean Abitibi Greenstone belt is the longest greenstone belt in the Superior Province of the Canadian Shield, consisting of diverse assemblages of basaltic to dacitic volcanic rocks with minor komatiites, and tonalitic to granodioritic intrusions, overlain by supracrustal sedimentary sequences. The greenstone belt hosts substantial volcanogenic massive sulfide (VMS) deposits (Percival *et al.,* 2012). From the central to southern areas of the catchment, the Ottawa River flows over the Proterozoic Grenville Province, composed of a series of accreted terranes consisting of high-grade paragneisses with minor amphibolites, granitic to granodioritic intrusions and volcanic rocks (e.g. Corriveau and Clark, 2005). The southernmost reaches of the ORB, where the Ottawa River flows from near Ottawa to Montreal before joining the St. Lawrence River, are dominated by Ordovician to Silurian sedimentary sequences of the St. Lawrence Platform (Sanford, 1993). Minor outcrops of the latter sequence are also present on the northern side of Lake Timiskaming.

Finally, there are also thick, unconsolidated sequences of marine clays and silts in the southern reaches of the ORB that were deposited as the former Champlain Sea drained back towards the Atlantic Ocean in response to isostatic rebound (Brydon and Patry, 1961). During the last deglaciation between 12 and 10 Ka, rising sea levels caused the Atlantic Ocean to extend inland from the Gulf of St. Lawrence along the St. Lawrence River, flooding the isostatically depressed St. Lawrence and Champlain Valleys as far as Deep River, Ontario. The inundation occurred between 13 and 9 Ka after the retreat of the Laurentide Ice Sheet (e.g. Parent and Occhietti, 1988; Cronin *et al.,* 2008) and was fed by drainage of glacial Lake Algonquin.

2.1.2 Anthropogenic activity (*Dams, Industry, Mining, Urban areas)*

The ORB catchment is host to a number of ore deposits and associated mining activity and a number of industries such as pulp and paper mills, urban centres, and the Ottawa River has been modified by a number of human-made dams along its course. All of these factors have the potential to anthropogenically modify natural geochemical signatures in the ORB, but their overall imprint on catchment-wide aquatic and soil geochemical signatures is very poorly defined.

The Abitibi greenstone belt and surrounding rocks host some of the largest Au and Cu-Zn deposits in the world. Currently there are 7 active mines between Rouyn-Noranda and Val D'Or (Madore and Caron, 2019), and there are over 100 abandoned mines in the Abitibi-Témiscamingue region, previously producing Au, Cu and Zn with minor amounts of Mo, Bi, Ag, Sb, Cd and U (MERN, 2017). Remediation work has been and is currently being carried out on a large number of these mining sites by the Ministère de l'Énergie et des Ressources Naturelles (MERN) reclamation initiative, which aims to reduce the environmental impact of abandoned mines, quarries, and acid mine drainage from tailing ponds and spoil heaps. Although molybdenite mining has not been prominent in the region, Mo

is primarily extracted as a by-product of the processing of Cu- and Au-porphyry ore deposits (Seo *et al.,* 2012); a report by SIDEX (2007) highlighted 225 deposits and closed mines for which Mo occurs or did occur in significant amounts, 103 of which produced Mo as a by-product, many of which occurred within the vicinity of Val D'Or.

In addition to mining, the Ottawa River is also affected by major industrial activity, and construction which disrupts the natural state of the river (Figure 1), the most noteworthy being Chalk River Laboratories, a nuclear research laboratory operated by Canadian Nuclear Laboratories (formerly Atomic Energy of Canada Ltd.). This laboratory was for many decades the world's leading producer of ^{99}Tc, a radioactive isotope used in medical imaging. Contamination of regions within the facility such as soil and groundwater has been detected following repeated incidents of radioactive waste leakage (e.g. Johnson *et al.,* 2015), though remediation works are taking place.

Paper and pulp factories, such as the one in Temiscaming, use a significant amount of water from the river and utilize chemicals such as NaOH, NaS_2, H_2SO_4 and HSO_3^-, and inorganic compounds such as ClO_3^- and various organo-chlorine compounds. According to a 2015 report by the Direction Générale des Politiques de l'Eau, each mill discharges between 0.3 and 0.54×10^6 m^3 of effluent per year, and from the two landfills containing waste from these mills, 75,000 and 971,000 m^3 of leachate is discharged annually. A growing demand for chlorine-free pulps have called for alternative bleaching methods including a molybdenum-activated hydrogen peroxide stage (Azevedo *et al.,* 2011), although it is not known whether such methods are practised within the factories of the ORB.

Currently there are over 50 major dams and hydroelectric generators throughout the Ottawa River and its tributaries, with 13 reservoirs containing more than 200 m^3 of water storage. The stagnancy of water within lakes and artificial reservoirs have the potential to create stratified water columns with sub-oxic to anoxic conditions in deeper regions. The build-up of organic matter within these oxygen-depleted zones may increase the potential scavenging of Mo from the water column and/or the precipitation of reduced Mo species (Malinovsky *et al.,* 2007).

2.2 Samples

Twenty-nine water samples were collected, following five sampling criteria. 1) At the site location of SLRS-4 from the reservoir at Chenaux, primarily to test the consistency of the Mo isotope signature over time at the same location (i.e., to allow comparison of new data to the SLRS-4 Mo isotope values obtained by Archer and Vance (2008)). This was the furthest downstream sample collected from the Ottawa River. 2) From different sections of hydroelectric dams, taken from the reservoir as well as directly below the dam and from a section upstream of the reservoir to evaluate any possible effects of deoxygenation within the reservoir and re-oxygenation in the turbulent waters below the dam. 3) From 4 major tributaries to the main Ottawa River: the River Noire, which is largely uncontrolled by

damming; the River Coulonge; the Petawawa River, which flows through the town of Petawawa and its industrial area including an open quarry site; and the Mattawa River, which flows out of Lake Trout near North Bay on the banks of Lake Nippissing. These samples record the contributions of some of the drainage systems to the main Ottawa River. 4) At and below the dam that exists directly at the pulp and paper mill in Temiscaming, as well as ca. 5 km upriver of any potential industrial influence from this industry. The latter sample is the furthest upstream sample collected from the Ottawa River. 5) From the main Ottawa River at several points between Chenaux and Temiscaming, including slow- and fast-flowing sections, to characterise the evolution of the water signal along the river's course before and after the addition of major tributaries and effects of industry and urban areas. Figure 1 shows all of the sampling locations within the ORB, and a further description of the sample localities can be found in Table 1.

3. Methods

3.1 Sample collection

Field work was carried out over 10 continuous days across July and August 2018, the driest months of the year based on the lowest average monthly discharge previously measured at Carillon of 1133 $m^3 s^{-1}$ (Ottawa River Regulation Planning Board, 2011). No extreme or unusual weather events were observed during this time, and discharge for the year followed the typical pattern observed throughout the previous decades.

3.1.1 Equipment and preparation

All 500 mL LDPE bottles used to collect filtered field samples for trace element and Mo isotope analyses were cleaned before use. This involved leaching the bottles in 0.5 M HNO_3 for 2 weeks, followed by rinsing and leaching with ultrapure MilliQ® for a further week. The bottles were again rinsed, closed with Parafilm® and sealed into two re-sealable plastic bags. Samples for major ion analysis were collected in separate 100 mL HDPE bottles cleaned in the same way.

3.1.2 Collection, filtration, and acidification

All field equipment was flushed with sample water before each sample collection and rinsed after sampling with deionized water. Collection was carried out via complete submersion of a designated collection bottle to limit floating particulates such as pollen or fluids from vehicles and other machinery. Samples were taken upstream of any platforms or boats from which samples were taken and bottom sediments that were disturbed were allowed to settle before collection began. Where direct filling of the

collection bottle was not practical, water was collected in a large pre-rinsed 10 L plastic bucket, from which the water sample was taken in the same manner. Water was filtered through a 0.45 μm pore diameter Nylon membrane using a hand pump, or electric pump for samples with a high suspended particle content. The filtered sample at each site was split into 2 separate 500 mL LDPE bottles labelled "A" and "B" for trace element and isotope analysis, as well as the 2 100 mL HDPE bottles for major ion analysis. *In-situ* analysis of river water pH, Eh, temperature and EC was carried out at each sample site.

Samples were shipped to the University of Bern immediately after field sampling. Bottle A for each sample was acidified within 2 weeks of arrival to ~0.5 M with HNO_3. Bottle B was acidified the same way ca. 6 months after field collection. Slight discolouration of the sample water appeared in Bottle B over time, but disappeared shortly after acidification. In both cases, acidification was done several weeks before sample preparation for analysis began to ensure chemical equilibrium at a low pH was reached. An aliquot of Bottle A was used for ultra-trace element analysis, as described in Babechuk *et al.* (2020); this work revealed no chemical effects from the 2-week delay in acidification. Adsorption of elements to PTFE surfaces is a possibility during long-term storage, though improbable for Mo due to its speciation primarily as a soluble oxyanion. All samples for Mo isotope analysis in this study were firstly undertaken from Bottle A (n=29), but 3 samples were selected for repeated analysis from Bottle B to confirm whether the different time period before acidification produced any change in the sample Mo isotope ratio (Table S1).

3.2 Sample preparation and analysis

3.2.1 Mo isotopes

All sample preparation and analysis for Mo isotopes were undertaken at the University of Bern. All acids used were triple-distilled in-house. Between 200 and 500 mL of water was evaporated in 60 mL screw-top Teflon® jars at 90°C, by repeated addition and drying of the sample in 40 mL segments to produce 30-50 ng of Mo. The samples were spiked with a 1:1 ^{97}Mo-^{100}Mo double-spike at this time and evaporated to homogenise the sample (Siebert *et al.,* 2001). Organic matter was oxidised by boiling the sample in 2 mL of 14 M HNO_3 at 130°C for 24 hours. The samples were then dissolved in 6 mL 4 M HCl + 0.1% Suprapur® H_2O_2 to keep Mo in its oxidised Mo(VI) state. Purification of Mo followed the method of Siebert *et al.* (2003) and Voegelin *et al.* (2009). Samples were first loaded onto pre-cleaned anion exchange columns (1.5 cm^3 Dowex 1x8 resin, 200-400 mesh). The samples were then passed over a cation exchange column (2 cm^3 Dowex 50x8 resin, 200-400 mesh) to remove Fe. Following evaporation of the Mo cut, remaining organic matter was oxidised by attacking and drying down twice with 100 μL of a 4:1 mixture of concentrated HNO_3 and H_2O_2. The river water certified reference material (CRM) SLRS-6 from the National Research Council Canada (NRC) and two procedural blanks

were prepared along with each batch of river water samples. Typical yields of this ion exchange procedure is >90%, owing to the very low matrix of the water samples. Typical procedural blanks contributed to ~1-3% of individual samples' total Mo, with higher contributions corresponding to lower total-Mo samples. The SLRS-6 bottles used were the same measured for ultra-trace elements in the study of Babechuk *et al.* (2020).

Molybdenum isotope data were obtained on a Thermo Scientific Neptune™ *Plus* Multicollector ICP-MS using a CETAC Aridus II™ desolvating nebuliser following the measurement procedure and data correction modified after Kurzweil *et al.* (2015a). Sample measurements were punctuated by the repeated measurement of a Johnson Matthey Mo ICP-MS calibration standard ($JMC_{Bern,}$ LOT no. 602332B) for instrumental mass bias correction, and U.S. National Institute of Standards and Technology (NIST) reference material SRM 3134 (LOT no. 891307). Results of reference materials and samples are reported as the per mil deviation from NIST SRM 3134 = +0.25‰ scale, in which JMC_{Bern} is the δ^{98}Mo = 0‰ reference point (Nägler *et al.,* 2014):

$$\delta^{98}Mo = \left[\left(\frac{\frac{^{98}Mo}{^{95}Mo}\ sample}{\frac{^{98}Mo}{^{95}Mo}\ NIST\ 3134 = +0.25‰}\right) - 1\right] \times 1000$$

Continuous analysis of NIST SRM 3134 over 1 year gave a mean difference to JMC_{Bern} of +0.27 ± 0.04‰ (2σ, n=23). A 2σ uncertainty of 0.11‰ calculated from repeated measurement of SLRS-6 (n=4) is the adopted uncertainty for sample unknowns; each measurement involved complete procedural preparation and SLRS-6 is closest in composition to the samples of this study. All uncertainties are reported as the 2 standard deviation (2σ) or 2 standard error for individual data points ($2\sigma_{\bar{x}}$). Possible interferences on masses 98 and 100 due to the presence of Ru was monitored by measurement of both ^{99}Ru and ^{101}Ru (Table S3; Figure S1). For 23 of the 37 measurements, interference correction of δ^{98}Mo signatures exceeded the 2σ value (Table S3). In this case no correction was applied, since uncorrected δ^{98}Mo signatures of standards analysed within the same sample run reproduced within uncertainty.

3.2.2 Major anions, cations and neutral species

Analysis of major cations and anions, total organic carbon (TOC), and alkalinity was carried out at the University of Bern. For major cations and anions, undiluted and unacidified samples were measured using a Metrohm 850 Professional Ion Chromatograph with an 858 Professional Sample Processor and fitted with Metrosep C4-150/4.0 columns. Calibration of the high and low peak areas was performed before sample analysis with in-house calibration solutions of 1-10 mg/L and 0.1-1 mg/L concentrations, respectively. Cation reference materials used were Sigma-Aldrich Multianion standard solution Nr. 89316 and two dilutions (1:20 and 1:100) of Multi Cation

Standard 2 for IC Nr. 93159. Cations were eluted with a mixture of 0.7 mM dipicolinic acid and 1.7 mM HNO_3 at a rate of 0.9 mL/min, for a total of 35 minutes at 45°C. Anion reference materials used were the Sigma-Aldrich multianion standard solution Nr. 89886 and two dilutions (1:200 and 1:2500) of the Romil PrimAg® IC Calibration mix A5, Art. M1014. Anions were eluted with 3.6 mM Na_2CO_3 at a flow rate of 0.7 mL/min for a total of 42 minutes at 45°C. A total of 50 µl of sample was introduced. Reference materials were analysed after 20 samples. Total OC was measured on a Multi N/C 2100S (Analytik Jena AG). Samples were acidified to a pH of <2 with 2 M HCl. The reference material Art. TOC1000-100 ML from Fluka was run alongside the samples. The samples were injected in 400 µl aliquots with an oven temperature of 750°C. Total alkalinity was measured with a Metrohm OMNIS Titrator with OMNIS titration software.

4. Results

All data pertaining to field measurements are displayed in Table 2, major ion data are shown in Table 3, and Mo isotope data are displayed in Table 4 along with selected trace element data from Babechuk *et al.* (2020). Data for several of the trace elements are converted to moles/volume (M) concentrations from the mass/mass concentrations originally reported in Babechuk *et al.* (2020). Major ion data are converted to meq/L for ease of comparison with global river data (Gaillardet *et al.,* 1999). Such conversions are shown in Table S2.

4.1 Field measurements and total dissolved solids

Surface water temperatures ranged from 19.7 to 28.2°C with an average of 24.7°C. The pH of river water samples are quasi-neutral to slightly alkaline from 7.1 to 8.3, excluding only one sample from the River Coulonge with a slightly acidic pH of 6.3. The four lakes are the most alkaline of all of the samples with pH ranging from 8.0 to 9.6. The highest measured pH was from a small, slightly upland lake fed only by rainwater. Specific conductance (SpC) is low in the tributaries, ranging from 23.6 to 45.2 µS/cm, and higher in the main river ranging from 50.8 to 64.7 µS/cm, and highest in the lakes from 47.5 to 93.9 µS/cm. Dissolved oxygen levels range from 3.5 to 15.7 mg/L, and Eh measurements range from 202.0 to 303.5 mV.

4.2 Mo concentration and isotope composition

4.2.1 SLRS-6 and repeatability

The average Mo concentration for SLRS-6 measured in this study was 2.06 ± 0.42 nM (n=4), which is identical within uncertainty to the certified concentration of 2.24 ± 0.18 nM (https://doi.org/10.4224/crm.2015.slrs-6) and the average of 2.06 ± 0.07 nM reported from 63 measurements from 7 separate SLRS-6 bottles by Babechuk *et al.* (2020), including the same bottles

measured here. The average concentration of SLRS-6 reported here is also identical within uncertainty to certified and compiled values of SLRS-4 (e.g. 2.17 ± 0.21 nM; Yeghicheyan *et al.*, 2001), including the 2 values reported by Archer and Vance (2008) of 2.00-2.17 nM. The Mo isotope composition of the SLRS-6 CRM has so far not been published. Our repeated analysis of SLRS-6 yielded an average δ^{98}Mo of +2.03 ± 0.11‰ (n=4, Figure 2; Table S4). Thus, the Mo isotope ratio of SLRS-6 is lighter than its precursor SLRS-4 with a δ^{98}Mo of +2.33‰ as reported by Archer and Vance (2008). This original value for SLRS-4 was normalised to a CPI Mo ICPMS standard and renormalisation to that used here (NIST SRM = +0.25‰) based on the comparisons of normalisation standards by Goldberg *et al.,* (2013), Greber *et al.,* (2012) and Nakagawa *et al.,* (2012). The uncertainty involved is below ±0.2‰. It is noted that SLRS-6 was taken downstream of SLRS-4 in the Ottawa River, i.e., near the city of Ottawa rather than Chenaux (see Babechuk *et al.* (2020) Figure 1 for locations of SLRS-4 and -6), and at a different point in time. Besides possible temporal variations, the difference between the two standards mimics the general downstream trend of decreasing δ^{98}Mo values.

The minimal variation in δ^{98}Mo between samples from bottles acidified after 2 weeks (Bottle A) and after 6 months (Bottle B) indicates that acidification at a later stage produced no significant Mo isotope fractionation effects (<+0.2‰; Table S1) even if any Mo did adsorb to the inner surface of storage bottles prior to acidification. The small variations observed are instead more likely attributed to inter-experiment differences (e.g. different standard batches, acids, instrument tuning). As such, the observed trends in the Ottawa River cannot be explained by inadequate sample storage effects.

4.2.2 Samples

The concentration of Mo [Mo] in all ORB samples is very low, with an average of 2.06 ± 2.61 nM (n=37, including repeated measurements) across the studied catchment area (Figure 4), compared to rivers analysed in other studies (e.g. the global compilation data in King and Pett-Ridge (2018) with an average of 28.7 ± 169.8 nM). These lower concentrations are comparable to some other major river systems, such as the Amazon (~4.3 nM; Archer and Vance, 2008), the Narmada (4.3 nM; Rahaman *et al.*, 2014) Icelandic rivers (~3.2 nM; Pearce *et al.*, 2010) as well as smaller river systems such as the Entlebuch, Switzerland (~1.9 nM; Neubert *et al.*, 2011)), or the Séjallières and Malaval stream waters of the French Massif Central (~2 nM; Voegelin *et al.*, 2012). The wide range of characteristics of these rivers with a low Mo content (e.g. bedrock, climate, weathering intensity, human activity) makes it challenging to distinguish a common control on Mo concentration.

The Ottawa River generally has a higher concentration than its tributaries and surrounding lakes with [Mo] ranging from 2.07 to 3.31 nM and decreasing downstream, with an average of 2.64 ± 0.63 nM (n=18). The tributaries Petawawa, Mattawa, Noire and Coulonge have a much lower average [Mo] of 0.90 ± 0.12 nM (n=3), 1.14 ± 0.33 nM (n=4), 0.58 ± 0.09 nM (n=4) and 0.80 ± 0.08 nM (n=2),

434 respectively. The 4 lakes studied here have a much wider range of concentrations ranging from 0.87 to
435 6.25 nM, giving an average of 2.94 ± 4.85 nM (n=6).

436 Molybdenum isotope compositions follow a similar pattern as [Mo], in that the Ottawa River
437 is isotopically heavier than the tributaries and lakes, and becomes isotopically lighter downstream
438 (Figure 3, 4). The δ^{98}Mo of the Ottawa River ranges from +2.02 to +3.13‰ with an average of +2.57 ±
439 0.84‰ (n=18), whereas each tributary is largely invariable in isotope composition with average δ^{98}Mo
440 values of +1.06 ± 0.09‰ (Petawawa, n=3), +0.88 ± 0.15‰ (Mattawa, n=4), +1.20 ± 0.27‰ (Noire,
441 n=4) and +1.09 ± 0.08‰ (Coulonge, n=2). Lake waters studied have similar isotope compositions to
442 the tributaries with an average of +1.21 ± 0.29‰ (n=6), albeit with more variation.

443 ## 4.3 Major elements, total organic carbon and alkalinity

444 Major ion concentrations are relatively low in all samples and many species were below the detection
445 limit of the ion chromatograph. In such cases, and if available, the elemental data reported in Babechuk
446 *et al.* (2020) from the same samples were used instead. Dissolved Ca^{2+} ranges from 129.2 to 176.0 µM
447 in the main river and is lower in the tributaries, between 56.6 and 82.8 µM. Magnesium is also lower in
448 the tributaries than in the main river, with concentrations between 22.1 and 48.6 µM and 56.1 and 75.6
449 µM, respectively. Dissolved Cl^- ranges in all samples between 5.5 and 76.9 µM, while SO_4^{2-} ranges from
450 44.7 to 62.2 µM in the main river, and is lower in the tributaries with values between 27.3 and 62.2 µM.
451 Total organic carbon (TOC) is also relatively low in all samples ranging from 5.6 to 10.2 mg/L,
452 including lake samples. Alkalinity as measured by HCO_3^- ranges from 23 to 32 mM in the main river
453 and is lower in the tributaries, between 12 and 18 mM.

454 # 5. Discussion

455 ## 5.1 Unusually isotopically heavy Mo isotope signatures in the ORB

456 The δ^{98}Mo of SLRS-4 (+2.33‰) reported by Archer and Vance (2008) remains one of the most
457 isotopically heavy signatures measured across all global rivers to date (e.g. King and Pett-Ridge, 2018).
458 The δ^{98}Mo values of samples collected at and immediately upstream of the SLRS-4 collection site
459 (SBB01, PDF01, RRR01 and CBM01) are very similar with values of +2.02 to +2.15‰ (Table 4). The
460 δ^{98}Mo value for SLRS-6, taken downstream of the latter samples is also similar at +2.03±0.11‰. This
461 study has revealed that δ^{98}Mo values in the Ottawa River reach even heavier isotope compositions
462 upstream, with the heaviest sample here (TMD01) at +3.13‰. Thus, not only is the earlier report from
463 Archer and Vance (2008) confirmed, but it now demonstrates that the unusually high δ^{98}Mo in the
464 Ottawa River is a widespread and consistent feature of the river.

Although the dissolved δ^{98}Mo signature of rivers across the globe are highly variable in comparison to one another and have been observed to display seasonal variation (Zeng *et al.,* 2019), the composition within single rivers and streams do not appear to vary significantly (i.e., within the range of 1‰) at any one time (e.g. King and Pett-Ridge, 2018; Nägler *et al.,* 2020; Pearce *et al.,* 2010). Individual streams within a catchment may display slightly different chemical signatures, an observation generally attributed to having different local sources of Mo (e.g. Voegelin *et al.,* 2012). However, it can be expected (e.g. Torres *et al.,* 2017), that the Mo content and isotope composition of the main river of a catchment would equal the sum of the composition of its tributaries and groundwater inputs (although it has been noted that tributaries with vastly differing solute concentrations may retain a heterogeneous chemical signature for several 10's of kilometres; Bouchez *et al.,* 2010). The δ^{98}Mo of the four tributaries in the ORB studied here fall within a narrow range between +0.82 and +1.29‰, values that are closer to other rivers measured globally. These individual tributaries are not observed to vary significantly downstream up to the point of emptying into the Ottawa River, and thus it is clear that they cannot explain the values up to 2.31‰ heavier in the latter (Table 4; Figure 3, 4). It then appears that either an additional process must be affecting the isotope composition of Mo exclusively in the main trunk of the catchment but not the tributaries, or an additional source of Mo must exist upstream of the measured tributaries that does not affect the rest of the catchment. More specifically, there must be a Mo source to the Ottawa River somewhere further north in the catchment that is isotopically heavier than the samples, either as a direct source or arising from the localized removal of light isotopes to generate a heavily-fractionated residual fluid.

Another unusual feature of the Ottawa River is that the Mo isotope composition becomes progressively lighter downstream, with a difference of over 1‰ between the uppermost and lowermost samples. This is in contrast to other studies demonstrating a uniform δ^{98}Mo composition along the course of the river with limited variation, or a composition that becomes progressively heavier downstream (Neubert *et al.,* 2011; Pearce *et al.,* 2010; Zeng *et al.,* 2019). The decrease in Mo concentration downstream could indicate the progressive removal of dissolved Mo from the water. However, most processes removing Mo (e.g. adsorption onto particulate surfaces) would be expected to favour the removal of light isotopes, driving the remaining dissolved Mo budget towards heavier isotope enrichment (e.g. Pearce *et al.,* 2010) – the opposite of what is observed.

Here, the potential causes of the unusually heavy isotopes of the river and downstream trend towards lighter compositions are evaluated in terms of potential inputs of Mo to, and outputs from, the ORB, and the possible processes driving catchment-scale isotope fractionation.

5.2 Dominant element sources in the ORB and relationship with Mo

The dissolved major element geochemistry (K^+, Mg^{2+}, Ca^{2+}, Na^+, SO_4^{2-}. HCO^-, Cl^-) of global river water is predominantly controlled by oxidative weathering, reflecting variable release of ions from the prevailing lithology of the drainage area, with additional minor contributions from atmospheric input. Modelling the contribution of the major ions derived from atmospheric input such as marine aerosols, delivered to the catchment by rainwater, is normally based on the molar $Z^{+/-}/Cl^-$ content of the river water samples (where $Z^{+/-}$ is the desired cation or anion; assuming Cl^- derives exclusively from atmospheric input; Gaillardet *et al.,* 1999; Millot *et al.,* 2002). The Cl^- content of the Ottawa River as well as the Mattawa River and the lowermost sample of the Petawawa River (PWL01, sampled downstream of the town of Petawawa), is higher than predicted by precipitation and runoff models by Millot *et al.,* (2002) for other major tributaries of the St. Lawrence River (15 μM). However, all samples are still generally low in Cl^- content compared to global large rivers (e.g. compilation in Gaillardet *et al.,* 1999) including the St. Lawrence River. Elevated Cl^- contents in rivers have been attributed to enhanced marine aerosol input, weathering of evaporites and saline groundwaters in granitic areas, as well as input from industry (including in the bleaching process of pulp and paper production) and urban areas where there is frequent road salting in the winter months (Gaillardet *et al.,* 1999; Yang *et al.,* 1996). The relatively low Cl/Na of all ORB samples in this study (<1) preclude the first three of these factors, which are characterised by Cl/Na of ~1.15, ~1 and ≫1, respectively (Gaillardet *et al.,* 1999). The slight excess Cl^- of the ORB (in comparison to other rivers) is therefore most likely attributed to minor urban and/or industrial inputs. Atmospheric Cl^- input is therefore set at a maximum of 15 μM, and this is used to correct for marine aerosol input to the major ion chemistry.

Initial impressions given by the generally low sum of dissolved major cations (TZ^+ (meq/L) = Ca^{2+} + Na^+ + K^+ + Mg^{2+}) throughout the basin (0.23-0.63 meq/L; Table S2) indicate the dominant control of weathering-resistant silicate bedrock. Gaillardet *et al.* (1999) discriminated between the geochemistry of global river waters in terms of their dominant lithological sources, namely silicates, carbonates and evaporites, via the co-variation of their molar Ca/Na, Mg/Na and HCO_3/Na ratios. As shown in Figure 5, the Ottawa River fits well within the context of global river waters, with good correlations between Ca/Na and Mg/Na, and HCO/Na, representing a mixture of river waters draining silicate- and carbonate-dominated lithologies. The relatively high Ca^{2+} content as a percentage of TZ^+ in both the Ottawa River and the tributaries (34-51%) points towards the influence of a Ca-rich lithological source. Telmer and Veizer (1999) conclude that the Ca^{2+} and Mg^{2+} content of the Ottawa River change from silicate-derived sources upstream from Lake Timiskaming to increasingly carbonate-derived sources downstream of the confluence with the River Noire as the proportion of Silurian-Ordovician rocks increase. However, some of the Ca^{2+} in upstream samples may derive from small pockets of carbonate on the north shore of Lake Timiskaming (Figure 1).

Although no Mo data is available for the specific rocks underlying the ORB, upper continental crustal composites such as post-Archaean Australian shale (PAAS), upper continental crust (UCC) or Mud from Queensland (MUQ) indicate that the concentration of Mo in continental rocks is on the order of 0.5-1.5 μg g^{-1} (e.g. Taylor and McLennan, 1985; Marx and Kamber, 2010). Carbonate rocks, on the other hand, have a much lower Mo content on the order of <100 ng g^{-1} (e.g. Eroglu *et al.,* 2015; Romaniello *et al.,* 2016; Voegelin *et al.,* 2009; Voegelin *et al.,* 2010), though are more susceptible to chemical weathering. Figure 6A-D shows the variation in Cl-normalised molar contents of major cations K^+, Mg^{2+} and Ca^{2+}, representing the contributions from felsic igneous rocks and carbonates, respectively, and the anion SO_4^{2-}, representing the contribution from sulfides, against Mo content (Wang *et al.,* 2015; Zeng *et al.,* 2019). The strong correlation between each of these elements and Mo in the tributaries inhibits the discrimination among clear dominant silicate-, carbonate- or sulfide-derived Mo using these relationships. Notably, however, the tributaries do not drain carbonate and the common correlation between K^+ and Ca^{2+} could be consistent with the Mo source being from igneous rocks rather than carbonates, with Ca^{2+} deriving from Ca-bearing minerals such as plagioclase in the igneous and metamorphic rocks of the area (Feng and Kerrich, 1992). In this case, the Mo could be released from its trace concentration in these minerals or from Ti-bearing minerals also common to these rock types. Notably, the ultra-trace element study of Babechuk *et al.* (2020) on the same samples indicated that several of the other trace elements signatures (e.g. REE+Y and HFSE) are best explained by a pervasively silicate-dominated source upstream of sampling. A silicate-dominated source of Mo is also agreeable with the conclusions of Telmer and Veizer (1999).

The Ottawa River samples do not plot on the same mixing line between silicate- and carbonate or Ca-rich igneous Mo sources as the tributaries, in terms of SO_4^- and K^+, and show no clear correlations, indicating a different dominant source upstream in the catchment. This change in dominant source becomes clear when the Mo is compared to the percentage contribution of K^+, $[Mg^{2+} + Ca^{2+}]$ and SO_4^{2-} to the ORB (Figure 6E-G). The differing relationship between the relative proportions of major ions, especially K^+ and $[Mg^{2+} + Ca^{2+}]$, and Mo content indicates a different source of Mo in the tributaries than in the Ottawa River, where Mo correlates more strongly with K^+ in the tributaries, and with $[Mg^{2+} + Ca^{2+}]$ in the Ottawa River. It then appears that the upstream Mo content is more closely associated with Ca and Mg in the Ottawa River, but, as will be argued based on the unusual Mo isotopic data, not necessarily indicating that the Mo is sourced from Ca-Mg-rich igneous rocks or the minor outcrops of carbonates.

5.3 Initial constraints on the upstream source of heavy Mo

In recent years, the low Mo concentration and heavy δ^{98}Mo signatures of many large rivers including the Ottawa River have been attributed to the retention of light isotopes in the weathering profile via

adsorption onto soil Fe, Mn and Al oxides, and subsequent release of isotopically heavy residual fluid (Archer and Vance, 2008; Goldberg *et al.,* 2009; Horan *et al.,* 2020; King *et al.,* 2018; King *et al.,* 2016; Marks *et al.,* 2015; Pearce *et al.,* 2010; Siebert *et al.,* 2015; Wang *et al.,* 2015; Wang *et al.,* 2018). Assuming equilibrium fractionation with calculated fractionation factors (α) of between 1.0008 and 1.0022 (Goldberg *et al.*, 2009), it is reasonable to attribute the Mo isotope composition of the tributaries (+0.82 - +1.29‰) to soil mechanisms either exclusively or in combination with bedrock influence, changing the signature of the Mo released from an assumed bedrock composition of between -0.5 and +0.8‰ (the average of igneous rocks; Greber *et al.,* 2014; Greber *et al.,* 2015; Horan *et al.,* 2020; Liu *et al.,* 2020; Pearce *et al.,* 2010; Siebert *et al.,* 2003; Voegelin *et al.,* 2014; Willbold *et al.,* 2016; Zhao *et al.,* 2016). This interpretation of the tributary δ^{98}Mo values is consistent with that of Babechuk *et al.* (2020) where redox-sensitive Ce anomalies and variations in the ratios of Mo, W, Th and U were attributed primarily to natural oxidative weathering processes in the ORB.

Conversely, the heavier Mo isotopic signature of the Ottawa River relative to the tributaries is difficult to reconcile with only natural processes operating in soils that retain isotopically light Mo, since factors such as soil types and climate are similar across the sampled areas of the ORB. Extreme variations in soil characteristics such as pH, organic content, and redox conditions have also not been shown to produce Mo isotope variations to the extent captured in the Ottawa River samples (Wang *et al.,* 2018; Siebert *et al.,* 2015), and even rivers such as the Amazon which drain Fe- and Al-oxide-rich laterites can have isotope compositions close to that of continental crust (Archer and Vance, 2008).

So far, the δ^{98}Mo signatures of the specific rocks underlying the ORB are not known. However, the anomalously heavy δ^{98}Mo signatures of the Ottawa River up to +3.13‰ exceed the known range of values for magmatic sulfides (-1.6 - +2.3‰; Breillat *et al.,* 2016; Greber *et al.,* 2011; Hannah *et al.,* 2007; Wieser and de Laeter, 2003), igneous rocks (-0.5-+0.8‰; Greber *et al.,* 2014; Greber *et al.,* 2015; Liu *et al.,* 2020; Pearce *et al.,* 2010; Siebert *et al.,* 2003; Voegelin *et al.,* 2014; Willbold *et al.,* 2016; Zhao *et al.,* 2016), and carbonates (up to ~+2.3‰; Czaja *et al.,* 2012; Eroglu *et al.,* 2015; Lu *et al.,* 2017; Thoby *et al.,* 2019; Voegelin *et al.,* 2009; Voegelin *et al.,* 2010; Wen *et al.,* 2011; Zhou *et al.,* 2011; Zhou *et al.,* 2015). Several experiments and field observations characterising the behaviour of Mo isotopes upon release from igneous and sulfide phases reported little to no fractionation (Neely *et al.,* 2018; Siebert *et al.,* 2003; Siebert *et al.,* 2015; Skierszkan *et al.,* 2016; Voegelin *et al.,* 2012), ruling out the preferential release of heavy isotopes from the source bedrock as a driver of these signatures. Thus, within the current knowledge of different continental bedrock signatures and soil processes, it is unlikely that the signatures of the Ottawa River are a reflection of bedrock and/or natural weathering processes alone.

5.4 Binary mixing in the Ottawa River

It is reemphasized that a large magnitude of downstream isotopic variation is not a ubiquitous feature of rivers (e.g. Neubert *et al.,* 2011; Neely *et al.,* 2018) and that the progressive downstream decrease in δ^{98}Mo accompanied by a decrease in [Mo] observed here in the Ottawa River is opposed to observations from other rivers. Although downstream Mo isotopic variation has been observed in rivers in Iceland (Pearce *et al.,* 2010) and China (Zeng *et al.,* 2019), and has been attributed to particle reactivity and removal of Mo onto colloids (Pearce *et al.,* 2010), these studies document a progressive downstream increase in δ^{98}Mo signatures. This latter trend is the expected response to preferentially adsorbing light Mo isotopes and producing a progressively heavier riverine isotope composition (Pearce *et al.,* 2010). Regardless, it has been suggested that Mo adsorption to riverine colloids does not represent an important sink for Mo nor contribute significantly to the overall Mo budget (Neubert *et al.,* 2011; Pearce *et al.,* 2010). This study finds excellent correlations between the downstream δ^{98}Mo signatures and the variations in HFSE and REE+Y concentrations and selected ratios (Nb/Ta, Zr/Hf, Th/U, Ce/Ce*) reported in Babechuk *et al.* (2020) (Figure 7). Although the latter elemental systematics were interpreted as indicators of downstream reactivity of dissolved species with colloids/fine particulates by Babechuk *et al.* (2020), the downstream progression towards light δ^{98}Mo signatures is counterintuitive to Mo removal from solution. Thus, we instead interpret these correlations without a causal relationship; the particle reactivity of the elemental tracers occurs progressively downstream as the trunk water of the Ottawa River is diluted by tributary inputs with a lower δ^{98}Mo. Accordingly, the downstream variations in [Mo] and δ^{98}Mo would record a binary mixing between the composition of the tributaries and an upstream source with higher [Mo] and higher δ^{98}Mo.

Here, we further explore and quantify the strong positive correlation between [Mo] and δ^{98}Mo of the main Ottawa River, and the progressive and consistent decrease in both parameters downstream, as a binary mixture between an unknown upstream source (further upstream of the uppermost sample taken near Temiscaming) with a very heavy Mo isotope signature (Source B) and tributaries (inc. small streams and groundwater) with lower [Mo] and δ^{98}Mo (Source A) that serves to progressively dilute upstream Source B during flow through the ORB (Figure 8). Considering that all samples (n=11) from the four tributaries analysed in this study are largely homogenous in terms of [Mo] (average 0.86 ± 0.50 nM) and δ^{98}Mo signatures (average +1.05 ± 0.31‰), the average tributary composition is taken as representative of Source A, the diluent. The exact composition of upstream Source B is more difficult to constrain, and all that can be said with certainty is that the [Mo] is greater than 2.88 nM and the δ^{98}Mo is greater than +3.1‰, the composition of sample TMU01 (Figure 8).

As is evident in Figure 8, downstream mixing/dilution in the Ottawa River is not uniform, and the data are divisible into two groups (Figures 4, 8), with a tight clustering of compositions in the upper part of the river from Temiscaming to Mattawa (Group 1), and a slight change in slope and greater

variation downstream of Mattawa (Group 2). The change between the groups occurs downstream of the confluence with the Mattawa River, the second of 16 major tributaries that flow into the Ottawa River (with only the Kipawa River upstream from this point). It is proposed that the slower rate of change in [Mo] and δ^{98}Mo in Group 1 reflects the less voluminous input of Mo to Lake Timiskaming and in the upper part of the Ottawa River via minor tributaries, streams, and groundwater, whereas the increased rate of mixing/dilution in Group 2 records the increased volume of these diluent sources (potentially with variable Mo compositions) being dispensed into the Ottawa River. Samples of Group 2 can be considered to fall on a mixing line constructed between Source A and the uppermost sample of Group 2 (KLR01, see supplementary information), whereas the samples of Group 1 do not, demonstrating this effect of increased dilution after the confluence of the Mattawa River.

Considering the vast area covered by the headwaters of the Ottawa River, which consists of an extensive network of streams and waterways interspersed with lakes and swamps, it is not only difficult to constrain a more specific composition, but also difficult to pinpoint an exact location of Source B. Nevertheless, one possible approximation is derived by extrapolation from the coupled trajectory of [Mo] and δ^{98}Mo in the Group 1 samples. In this approximation, we consider Source B as the northernmost point of Lake Timiskaming, the furthest upstream point of a similar discharge that is most clearly traceable (Figure 1). This point is ~100 km upstream of TMU01, and using the rate of change in [Mo] and δ^{98}Mo observed in Group 1 corresponds to a composition with [Mo] of ~3.2 nM and δ^{98}Mo of ~+3.5‰ (Figure 8).

The binary mixing model presented in Figure 8 is undoubtedly simplified from the natural complexities of the ORB and includes a wide range of potential compositions and locations of Source B. Nonetheless, the unusual Source B Mo isotope composition, which has yet to be identified in the ORB and is beyond the values resulting from natural fractionation processes in other catchments, remains a requirement. This observation invited the consideration of other potential non-natural sources of Mo to the Ottawa River, or otherwise any potential processes affecting the natural Mo cycle.

5.5 Anthropogenic processes or sources of Mo

An increasingly appreciated component of the Mo surface cycle is that of anthropogenic Mo input or artificially induced/enhanced fractionation of Mo in "human-made" environments. Here, we consider all possible disruptions to the natural Mo cycle in the ORB, starting with those situated in the sampled areas of the catchment. The sampling strategy of this study was partly motivated by the potential influence of industry and infrastructure such as hydroelectric dams on the δ^{98}Mo signature of the Ottawa River in comparison to tributaries that are not modified and are further away from industry. The downstream trend seen in the δ^{98}Mo signature of the Ottawa River does not correspond with any of the dams nor the industrial regions of the river. The nuclear research laboratory at Chalk River (Figure 1) is also noteworthy since the production of ^{99}Tc is linked to ^{99}Mo, which would form an isobaric

interference with ^{99}Ru that is potentially relevant to corrections to the MC-ICP-MS data (Section 3.2.1); mass 99 is used to correct the Mo isotope masses assuming all of the mass is Ru and it has a natural ratio to ^{101}Ru. This interference correction showed no indication of an influence from non-natural mass 99 isotopes traceable to sampling location (Figure S1; Table S3), and correction using mass 101 in place of mass 99 produced identical δ^{98}Mo values within 0.02‰.

The heaviest δ^{98}Mo signatures found in the Ottawa River are ~180 km upstream of Chalk River and also upstream of the pulp and paper factory at Temiscaming. Thus, the unusually heavy Mo isotope signature of Source B in the binary mixing model of the Ottawa River data (Section 5.4) must originate in the northern reaches of the ORB, where mining activity in the regions of Rouyn-Noranda and Val D'Or stand out as plausible options. Consequently there is growing precedent to evaluate the influence of mining activity on the surface Mo cycle of the ORB.

Acid mine drainage from molybdenite mines extremely enriched in Mo has so far been identifiable in rivers by unusually high Mo content of the river water, such as that of Antamina and Thompson Creek Mines (Skierszkan *et al.,* 2016; Skierszkan *et al.,* 2017; Skierszkan *et al.,* 2019) with Mo contents of mine runoff and drainage waters on the order of >>3000nM. The molybdenite mining-affected Clear Creek river, Colorado, with Mo concentrations of around 500 nM (Archer and Vance, 2008), is the most Mo-enriched river included in the global river water compilation of King and Pett-Ridge (2018), 3 to 4 times higher than the next most concentrated rivers, namely the Sikkim, India (up to 139 nM) and the Huanghe, China (up to 123 nM). However, even with highly elevated [Mo], most mine drainage and clearly mining-affected river water are typically characterised by a Mo isotope composition within the range of continental crustal signatures. Therefore, the δ^{98}Mo alone does not directly fingerprint an anthropogenic source of Mo linked to mining, and, at first glance, the overall low [Mo] of the Ottawa River does not directly support a mining influence in the ORB, as per the conclusions of Archer & Vance (2008).

Anthropogenic disturbance to the natural lake sediment δ^{98}Mo signatures of two lakes in Quebec (Figure 1) has previously been linked to aerosol emissions from a large smelter in Rouyn-Noranda active in the 20th Century (Chappaz *et al.,* 2008; Chappaz *et al.,* 2012) about 80 km northeast of Lake Timiskaming, in which a distinctive anthropogenic δ^{98}Mo signature in the uppermost layers of lake sediments of Lac Tantare was linked to the above-mentioned smelter, ~200 km away from Rouyn-Noranda. Fractionation of Mo during the smelting process was not inferred from the lake sediment data, which was found to be within the range of previously-analysed molybdenite ores from the region (~+0.2‰; Breillat *et al.*, 2016). Although neither widespread aerosol emissions nor direct input of mine discharge can directly account for the Source B signature inferred from the Ottawa River data, the study of the smelter emissions at Rouyn-Noranda nonetheless demonstrate the wide-reaching effects of this localised anthropogenic source that could include an indirect influence on the ORB.

706 To explain both the low [Mo] and unusually heavy δ^{98}Mo of Source B, our preferred
707 interpretation involves the convergence of both a Mo source, possibly linked to mine wastes, and
708 unnatural levels of Mo removal with Rayleigh-type fractionation generating high δ^{98}Mo values. Recent
709 studies carried out by Skierszkan *et al.* (2016), Skierszkan *et al.* (2017) and Skierszkan *et al.* (2019)
710 demonstrated a systematic offset between the composition of pond water draining from waste rock
711 storage facilities relative to the host waste rock material and the molybdenite ore in two molybdenite
712 mines in the USA (Thompson Creek Mine, Idaho) and Peru. The δ^{98}Mo values of the oxic pond waters
713 reached +2.6‰, up to 1.6‰ heavier than the original source rock. These authors attribute most of the
714 isotopic fractionation to the human-made waste rock environments, in which the precipitation of Fe-
715 (oxyhydr)oxides in oxic drainage ponds following the discharge of anoxic, Fe(II)-rich seepage from
716 mine tailings resulted in enhanced adsorption of isotopically light Mo(VI). Further fractionation
717 between the source of Mo (molybdenite) and the drainage water was also attributed to further adsorption
718 of Mo onto pyrite and other minerals stable in anoxic zones of the waste rock storage facility prior to
719 release, as well as the repeated reductive dissolution of oxides. Skierszkan *et al.* (2019) calculated a
720 fractionation of 1‰ between the aqueous Mo phase and the bedrock source of Mo due to adsorption
721 primarily onto ferrihydrite minerals, which is close to the experimentally-determined fractionation of
722 1.1‰ by Goldberg *et al.* (2009). Here, we advocate for a similar sequence of processes developing the
723 composition of Source B in the upstream regions of the ORB, which require a net $\Delta^{98}Mo_{oxide\text{-}aqueous}$ of at
724 least ~2‰ δ^{98}Mo from the natural background of the tributaries (+1.1‰) to reach the minimum isotopic
725 composition of the unknown Source B (+3.1‰).

726 Starting with different assumed Mo source compositions, similar to that of Thompson Creek
727 ([Mo]=3554 nM, δ^{98}Mo=0.69‰; Skierszkan *et al.* (2019)), Clear Creek ([Mo]=508 nM, δ^{98}Mo=0.24‰;
728 Skierszkan *et al.* (2019)), or the Don Rouyn molybdenite ore (assumed theoretical [Mo]=100 nM;
729 measured δ^{98}Mo=0.2‰; Breillat *et al.,* 2016), Rayleigh fractionation lines for aqueous Mo after removal
730 of Mo(VI) by oxides are shown in Figure 8. These modelled fractionation pathways are derived from:

731 $$\delta_B = [(\delta_{init} + 1000)f^{\alpha-1}] - 1000$$

732 where δ_B denotes the δ^{98}Mo composition of the remaining aqueous Mo (evolving to produce Source B),
733 δ_{init} denotes the initial δ^{98}Mo composition of aqueous Mo, f denotes the fraction of Mo remaining in the
734 water and α is the fractionation factor between the water and the adsorbent phase (Skierszkan *et al.,*
735 2016; Weiss *et al.,* 2008) here assumed to be 1‰ as per Skierszkan *et al.* (2019). We envisage the
736 fractionation being facilitated by oxic waters related to uncontained acid mine drainage or oxic areas of
737 the numerous sulfide tailing ponds within the Abitibi mining region (Benzaazoua *et al.,* 2000; specific
738 locations and names of mines withheld). Additionally, adsorption of Mo onto pyrite and other stable
739 sulfides within anoxic tailing ponds with a fractionation of up to 2.9‰ for pyrite (Bostick *et al.,* 2003)
740 may induce even greater fractionation of the Mo source and retention prior to discharge into oxic waters.

Waters processed through the Rayleigh-type fractionation of Mo isotopes with removal of >96 % of the initial aqueous Mo, as is possible in mine influenced environments, can develop the low [Mo] and high δ^{98}Mo signatures needed for Source B (Figure 8). Assuming the binary mixing model involving further downstream dilution of Source B by natural Mo sources in the ORB (represented by the tributaries; Source A) is valid, the Rayleigh fractionation step can also further constrain a probable range of Source B compositions in terms of [Mo] and δ^{98}Mo (Figure 8). These results are consistent with Babechuk *et al.* (2020) noting that Mo/W ratios in the same Ottawa River samples imply fractionation of the ratio from crustal source values with W>Mo retained on (oxyhyr)oxides in soils or throughout upstream riverine systems. However, this inference of mining activities playing a role in anthropogenic disruption to the Mo geochemistry of the Ottawa River should be substantiated with further work. Such work should target the upper reaches of the catchment, ideally at potential sinks for Mo in, and adjacent to, mining waste rock sites, as well as aim to further delineate the riverine signatures across the headwater network.

5.6 Implications for the modern global Mo riverine flux and its application in paleoredox studies

The most up-to-date modern average riverine δ^{98}Mo composition calculated from the literature data compiled by King and Pett-Ridge (2018; Figure 4) currently stands at +0.8‰. This, and all previous estimates since the initial work by Archer and Vance (2008), include the anomalously heavy Mo isotope signature of the Ottawa River under the assumption that it reflects natural Mo removal processes in the weathering environment (Archer and Vance, 2008). This study confirms the anomalous δ^{98}Mo signature of the Ottawa River, but more clearly documents that the signature is decoupled from natural weathering processes. The data and modelling of this study suggest that the Ottawa River is influenced by an as of yet unknown point source (or sources) producing the unusually heavy Mo isotopes signatures that is apparently capable of surviving through downstream dilution. The relatively low [Mo] of waters in the ORB likely render them considerably more susceptible to overprinting of their natural isotope signatures by even a small influx of an unnatural component.

Assuming our inference of an unnatural component in the northern reaches of the ORB is correct, the spatial extent of the effect from this source throughout the ORB is striking, with residual unusually heavy Mo isotope signatures sustained for at least ~350 km downstream. Other metal abundances in the Ottawa River (e.g. the concentrations in SLRS-6) do not reveal an obvious imprint from mine wastes in the northern reaches of the catchment, but could reflect their particle-reactive nature and sequestration in particulates in northern areas of the ORB. As such, the results would indicate that non-natural fractionation mechanisms could be a cryptic, yet integrated component of the modern Mo cycle. An important consequence of this interpretation is the potential wide-reaching effects of unnatural Mo sources in other river catchments. It is known that a large number of rivers worldwide are

affected directly by mining activities and heavy metal pollution (e.g. Malm *et al.,* 1990; Pagnanelli *et al.,* 2004; Silva *et al.,* 2013; Smolders *et al.,* 2003; Solongo *et al.,* 2018), and the more wide-reaching, catchment-scale effects from anthropogenic aerosols such as that from smelters has already been shown (Chappaz *et al.,* 2008; Chappaz *et al.,* 2012). In terms of Mo geochemistry, however, recognition of anthropogenically influenced rivers has, to date, relied on screening for unusually high [Mo]. Further, studies of acid mine drainage-related, artificially-induced Mo isotope fractionation has largely focused on localised effects within the specific mine environment (i.e., within waste rock storage facilities, drainage water and drainage ponds; Skierszkan *et al.,* 2016; Skierszkan *et al.,* 2017; Skierszkan *et al.,* 2019). The catchment-scale disruption to δ^{98}Mo in the ORB inferred in this study suggests further work is needed in catchment areas downstream from well-characterized point sources of heavy Mo isotopes to better understand how pervasive such signatures can be prior to buffering by natural δ^{98}Mo signatures.

The inclusion of potential non-natural signatures in the global modern river average δ^{98}Mo signature may become important in the context of paleoredox studies, specifically in the use of the modern Mo flux to the ocean in mass balance models as an analogue for that of the past. Estimates of past Mo delivery to the ocean are modelled on the modern global average riverine Mo flux and δ^{98}Mo composition (e.g. Kendall *et al.*, 2011) under the assumption that the modern riverine Mo flux is "pristine" and reflects that of the past. However, this study challenges assumptions that major river systems are recording pristine δ^{98}Mo signatures when based on inferences from Mo content, other trace metal data, or distance from potential anthropogenic sources. It is noted that the Ottawa River is only one large river constituting 0.2% of the global riverine input of freshwater to the ocean, and that the removal of Ottawa River data does not significantly alter the average global δ^{98}Mo signature calculated from the literature data in Figure 4. Nevertheless, the Ottawa River exemplifies that until further study has been conducted to verify purely natural riverine processes, some major rivers may be unsuitable for inclusion in future estimates of the global average Mo riverine flux, if the average is to be applied for paleoredox modelling. Based on the results of this study, it is proposed that the Ottawa River values should be excluded and that a compilation and averaging of smaller, more remote catchments without direct influence of human activity may provide a more reliable estimate.

6. Conclusion

This study documents the first catchment-scale δ^{98}Mo characterisation of the ORB in Canada. The Ottawa River, the trunk stream of the catchment, was previously identified as having a globally anomalous heavy Mo isotope signature via the certified reference material series SLRS from National Research Council Canada (Archer and Vance, 2008). The new data reported here confirm the unusually high δ^{98}Mo of the Ottawa River and extend this up to a maximum of +3.13‰, the heaviest river water

signature reported to date. The Ottawa River values stand in contrast to four major tributaries in the central area of the catchment with isotope compositions characterised by δ^{98}Mo more typical of global rivers. Furthermore, the δ^{98}Mo signature of the Ottawa River becomes progressively lighter downstream accompanied by a decreasing Mo content, a behaviour which is not observed in ORB tributaries and so far not been documented in any other river. The unique behaviour of the Ottawa River δ^{98}Mo signatures cannot be readily explained by underlying bedrock signatures, fractionation mechanisms related to weathering and soil processes, or downstream particle reactivity. Instead, trends are more consistent with the mixing/dilution of an even isotopically heavier source of Mo in the upper reaches of the Ottawa River with the natural bedrock- and/or weathering-controlled river water Mo source represented by the tributaries. It is proposed here that the unusually heavy Mo isotope signature upstream of sampling is indirectly related to the diverse mining district of the Abitibi-Temiscaming region in the headwaters of the Ottawa River. Mine wastes and tailings would provide a possible mechanism for developing an extreme, unnatural Mo isotopic fractionation signal, similar to what has been previously shown to occur in waste rock storage facilities in molybdenite mines. This proposal of an anthropogenic source of the unusually heavy Mo isotopic composition of the Ottawa River invites further work in the upper reaches of the ORB to better define Mo sources and isotopic fractionation processes. Further, the far-reaching downstream distribution of the anthropogenic signature (>350 km) was a surprising finding that may also be relevant to other catchments. This study illustrates that the Ottawa River should not be included in future compilations of global riverine δ^{98}Mo when it is to be applied for paleo-redox modelling and, similarly, that seemingly pristine river waters must be interpreted with caution until unnatural Mo sources or controls on isotope signatures can be refuted.

Acknowledgements

This research was supported financially by the Swiss National Science Foundation (grant #160034), and in part through a Natural Sciences and Engineering Research Council of Canada (NSERC) Discovery Grant (RGPIN-2017-05028). Special thanks to A.L. Nägler for assistance in field work and sample collection, and we thank N. Waber and laboratory assistants at the Institute of Geological Sciences, University of Bern for support in sample preparation and analysis. We extend our thanks to E. Skierszkan and F. Kurzweil, as well as guest editor R. Schoenberg for their positive and constructive reviews that helped improve this manuscript.

References

Alberta Environmental and Sustainable Resource Development (ESRD) 2014, Environmental Quality Guidelines for Alberta Surface Waters. Water Policy Branch, Policy Division, Edmonton. 48

842 Anbar, A.D., Duan, Y., Lyons, T.W., Arnold, G.L., Kendall, B., Creaser, R.A., Kaufman, A.J.,
843 Gordon, G.W., Scott, C., Garvin, J., Buick, R., 2007. A Whiff of Oxygen Before the Great
844 Oxidation Event? Science 317, 1903-1906.

845 Archer, C., Vance, D., 2008. The isotope signature of the global riverine molybdenum flux and anoxia
846 in the ancient oceans. Nature Geoscience 1, 597.

847 Arnold, G.L., Anbar, A.D., Barling, J., Lyons, T.W., 2004. Molybdenum Isotope Evidence for
848 Widespread Anoxia in Mid-Proterozoic Oceans. Science 304, 87-90.

849 Arnórsson, S., Óskarsson, N., 2007. Molybdenum and tungsten in volcanic rocks and in surface and
850 <100°C ground waters in Iceland. Geochimica et Cosmochimica Acta 71, 284-304.

851 Azevedo, M.A.B., Pasa, V.M.D., Hämäläinen, H., Mounteer, A.H., de Oliveira, R.C., Colodette, J.L.,
852 2011. ECF bleaching with molybdenum activated acid peroxide and its impact on eucalyptus pulp
853 properties and effluent quality. Natural Resources 2, 61.

854 Babechuk, M.G., O'Sullivan, E.M., McKenna, C.A., Rosca, C., Nägler, T.F., Schoenberg, R.,
855 Kamber, B.S., 2020. Ultra-trace Element Characterization of the Central Ottawa River Basin Using
856 a Rapid, Flexible, and Low-Volume ICP-MS Method. Aquatic Geochemistry 26. 327-374.

857 Baldwin, G.J., Nägler, T.F., Greber, N.D., Turner, E.C., Kamber, B.S., 2013. Mo isotopic
858 composition of the mid-Neoproterozoic ocean: An iron formation perspective. Precambrian
859 Research 230, 168-178.

860 Barling, J., Anbar, A.D., 2004. Molybdenum isotope fractionation during adsorption by manganese
861 oxides. Earth and Planetary Science Letters 217, 315-329.

862 Barling, J., Arnold, G.L., Anbar, A.D., 2001. Natural mass-dependent variations in the isotopic
863 composition of molybdenum. Earth and Planetary Science Letters 193, 447-457.

864 Benzaazoua, M., Bussière, B., Kongolo, M., McLaughlin, J., Marion, P., 2000. Environmental
865 desulfurization of four Canadian mine tailings using froth flotation. International Journal of Mineral
866 Processing 60, 57-74.

867 Beutel, M.W., 2003. Hypolimnetic Anoxia and Sediment Oxygen Demand in California Drinking
868 Water Reservoirs. Lake and Reservoir Management 19, 208-221.

869 Bostick, B.C., Fendorf, S., Helz, G.R., 2003. Differential Adsorption of Molybdate and
870 Tetrathiomolybdate on Pyrite (FeS_2). Environmental Science & Technology 37, 285-291.

871 Bouchez, J., Lajeunesse, E., Gaillardet, J., France-Lanord, C., Dutra-Maia, P., Maurice, L., 2010.
872 Turbulent mixing in the Amazon River: The isotope memory of confluences. Earth and Planetary
873 Science Letters 290, 37-43.

874 Breillat, N., Guerrot, C., Marcoux, E., Négrel, P., 2016. A new global database of δ^{98}Mo in
875 molybdenites: a literature review and new data. Journal of Geochemical Exploration 161, 1-15.

876 Brydon, J., Patry, L., 1961. Mineralogy of Champlain Sea sediments and a Rideau clay soil profile.
877 Canadian Journal of Soil Science 41, 169-181.

878 Chappaz, A., Gobeil, C., Tessier, A., 2008. Geochemical and anthropogenic enrichments of Mo in
879 sediments from perennially oxic and seasonally anoxic lakes in Eastern Canada. Geochimica et
880 Cosmochimica Acta 72, 170-184.

881 Chappaz, A., Lyons, T.W., Gordon, G.W., Anbar, A.D., 2012. Isotope Fingerprints of Anthropogenic
882 Molybdenum in Lake Sediments. Environmental Science & Technology 46, 10934-10940.

883 Cheng, M., Li, C., Zhou, L., Xie, S., 2015. Mo marine geochemistry and reconstruction of ancient
884 ocean redox states. Science China Earth Sciences 58, 2123-2133.

885 Czaja, A.D., Johnson, C.M., Roden, E.E., Beard, B.L., Voegelin, A.R., Nägler, T.F., Beukes, N.J. and
886 Wille, M., 2012. Evidence for free oxygen in the Neoarchean ocean based on coupled iron–
887 molybdenum isotope fractionation. Geochimica et Cosmochimica Acta, 86, 118-137.

888 Collier, R.W., 1985. Molybdenum in the Northeast Pacific Ocean1. Limnology and Oceanography 30,
889 1351-1354.

890 Corriveau, L., Clark, T., 2005. Introduction to the Grenville Province: a geological and mineral
891 resources perspective derived from government and academic research initiatives 1, 2. Canadian
892 Journal of Earth Sciences 42, 1637-1642.

893 Cronin, T.M., Manley, P.L., Brachfeld, S., Manley, T.O., Willard, D.A., Guilbault, J.P., Rayburn,
894 J.A., Thunell, R., Berke, M., 2008. Impacts of post-glacial lake drainage events and revised
895 chronology of the Champlain Sea episode 13–9 ka. Palaeogeography, Palaeoclimatology,
896 Palaeoecology 262, 46-60.

897 Dai, A., Trenberth, K.E., 2002. Estimates of Freshwater Discharge from Continents: Latitudinal and
898 Seasonal Variations. Journal of Hydrometeorology 3, 660-687.

899 Erickson, B.E., Helz, G.R., 2000. Molybdenum(VI) speciation in sulfidic waters:: Stability and
900 lability of thiomolybdates. Geochimica et Cosmochimica Acta 64, 1149-1158.

901 Eroglu, S., Schoenberg, R., Wille, M., Beukes, N., Taubald, H., 2015. Geochemical stratigraphy,
902 sedimentology, and Mo isotope systematics of the ca. 2.58–2.50 Ga-old Transvaal Supergroup
903 carbonate platform, South Africa. Precambrian Research 266, 27-46.

Feng, R., Kerrich, R., 1992. Geochemical evolution of granitoids from the Archean Abitibi Southern Volcanic Zone and the Pontiac subprovince, Superior Province, Canada: Implications for tectonic history and source regions. Chemical Geology 98, 23-70.

Gaillardet, J., Dupré, B., Louvat, P., Allègre, C.J., 1999. Global silicate weathering and CO2 consumption rates deduced from the chemistry of large rivers. Chemical Geology 159, 3-30.

Goldberg, S., Forster, H., Godfrey, C., 1996. Molybdenum adsorption on oxides, clay minerals, and soils. Soil Science Society of America Journal 60, 425-432.

Goldberg, T., Archer, C., Vance, D., Poulton, S.W., 2009. Mo isotope fractionation during adsorption to Fe (oxyhydr)oxides. Geochimica et Cosmochimica Acta 73, 6502-6516.

Goldberg, T., Gordon, G., Izon, G., Archer, C., Pearce, C.R., McManus, J., Anbar, A.D., Rehkämper, M., 2013. Resolution of inter-laboratory discrepancies in Mo isotope data: an intercalibration. Journal of Analytical Atomic Spectrometry 28, 724-735.

Greaney, A.T., Rudnick, R.L., Gaschnig, R.M., Whalen, J.B., Luais, B., Clemens, J.D., 2018. Geochemistry of molybdenum in the continental crust. Geochimica et Cosmochimica Acta 238, 36-54.

Greber, N.D., Hofmann, B.A., Voegelin, A.R., Villa, I.M., Nägler, T.F., 2011. Mo isotope composition in Mo-rich high- and low-T hydrothermal systems from the Swiss Alps. Geochimica et Cosmochimica Acta 75, 6600-6609.

Greber, N.D., Siebert, C., Nägler, T.F. and Pettke, T., 2012. $\delta^{98/95}$Mo values and molybdenum concentration data for NIST SRM 610, 612 and 3134: Towards a common protocol for reporting Mo data. Geostandards and Geoanalytical Research, 36(3), 291-300.

Greber, N.D., Pettke, T. and Nägler, T.F., 2014. Magmatic–hydrothermal molybdenum isotope fractionation and its relevance to the igneous crustal signature. Lithos, 190, 104-110.

Greber, N.D., Puchtel, I.S., Nägler, T.F. and Mezger, K., 2015. Komatiites constrain molybdenum isotope composition of the Earth's mantle. Earth and planetary science letters, 421, 129-138.

Hannah, J., Stein, H., Wieser, M., De Laeter, J., Varner, M., 2007. Molybdenum isotope variations in molybdenite: Vapor transport and Rayleigh fractionation of Mo. Geology 35, 703-706.

Helz, G.R., Bura-Naki, E., Mikac, N., Ciglenečki, I., 2011. New model for molybdenum behavior in euxinic waters. Chemical Geology 284, 323-332.

Helz, G.R., Miller, C.V., Charnock, J.M., Mosselmans, J.F.W., Pattrick, R.A.D., Garner, C.D., Vaughan, D.J., 1996. Mechanism of molybdenum removal from the sea and its concentration in black shales: EXAFS evidence. Geochimica et Cosmochimica Acta 60, 3631-3642.

936 Horan, K., Hilton, R.G., McCoy-West, A.J., Selby, D., Tipper, E.T., Hawley, S., Burton, K.W., 2020.
937 Unravelling the controls on the molybdenum isotopic composition of rivers. Geochemical
938 perspectives letters. 13, 13-18.

939 IGBP-DIS, 1998. SoilData(V.0) A program for creating global soil-property databases, IGBP Global
940 Soils Data Task, France.

941 Johnson, C., Lowrey, J., Biegalski, S. and Haas, D., 2015. Regional transport of radioxenon released
942 from the Chalk River Laboratories medical isotope facility. Journal of Radioanalytical and Nuclear
943 Chemistry, 305(1), 207-212.

944 Kashiwabara, T., Takahashi, Y., Tanimizu, M., Usui, A., 2011. Molecular-scale mechanisms of
945 distribution and isotopic fractionation of molybdenum between seawater and ferromanganese
946 oxides. Geochimica et Cosmochimica Acta 75, 5762-5784.

947 Kasper, D., Forsberg, B.R., Amaral, J.H.F., Leitão, R.P., Py-Daniel, S.S., Bastos, W.R., Malm, O.,
948 2014. Reservoir Stratification Affects Methylmercury Levels in River Water, Plankton, and Fish
949 Downstream from Balbina Hydroelectric Dam, Amazonas, Brazil. Environmental Science &
950 Technology 48, 1032-1040.

951 Kendall, B., Gordon, G.W., Poulton, S.W., Anbar, A.D., 2011. Molybdenum isotope constraints on
952 the extent of late Paleoproterozoic ocean euxinia. Earth and Planetary Science Letters 307, 450-460.

953 Kendall, B., Dahl, T.W., Anbar, A.D., 2017. The stable isotope geochemistry of molybdenum.
954 Reviews in Mineralogy and Geochemistry 82, 683-732.

955 King, E.K., Perakis, S.S., Pett-Ridge, J.C., 2018. Molybdenum isotope fractionation during adsorption
956 to organic matter. Geochimica et Cosmochimica Acta 222, 584-598.

957 King, E.K., Pett-Ridge, J.C., 2018. Reassessing the dissolved molybdenum isotopic composition of
958 ocean inputs: The effect of chemical weathering and groundwater. Geology 46, 955-958.

959 King, E.K., Thompson, A., Chadwick, O.A., Pett-Ridge, J.C., 2016. Molybdenum sources and
960 isotopic composition during early stages of pedogenesis along a basaltic climate transect. Chemical
961 Geology 445, 54-67.

962 Konhauser, K.O., Lalonde, S.V., Planavsky, N.J., Pecoits, E., Lyons, T.W., Mojzsis, S.J., Rouxel,
963 O.J., Barley, M.E., Rosìere, C., Fralick, P.W., Kump, L.R., Bekker, A., 2011. Aerobic bacterial
964 pyrite oxidation and acid rock drainage during the Great Oxidation Event. Nature 478, 369.

965 Kurzweil, F., Drost, K., Pašava, J., Wille, M., Taubald, H., Schoeckle, D., Schoenberg, R., 2015a.
966 Coupled sulfur, iron and molybdenum isotope data from black shales of the Teplá-Barrandian unit

argue against deep ocean oxygenation during the Ediacaran. Geochimica et Cosmochimica Acta 171, 121-142.

Kurzweil, F., Wille, M., Schoenberg, R., Taubald, H., Van Kranendonk, M.J., 2015b. Continuously increasing δ^{98}Mo values in Neoarchean black shales and iron formations from the Hamersley Basin. Geochimica et Cosmochimica Acta 164, 523-542.

Lawrence, M.G., Greig, A., Collerson, K.D., Kamber, B.S., 2006. Rare Earth Element and Yttrium Variability in South East Queensland Waterways. Aquatic Geochemistry 12, 39-72.

Lehmann, B., Nägler, T.F., Holland, H.D., Wille, M., Mao, J., Pan, J., Ma, D., Dulski, P., 2007. Highly metalliferous carbonaceous shale and Early Cambrian seawater. Geology 35, 403-406.

Liermann, L.J., Mathur, R., Wasylenki, L.E., Nuester, J., Anbar, A.D. and Brantley, S.L., 2011. Extent and isotopic composition of Fe and Mo release from two Pennsylvania shales in the presence of organic ligands and bacteria. Chemical Geology, 281(3-4), 167-180.

Liu, J.-H., Zhou, L., Algeo, T.J., Wang, X.-C., Wang, Q., Wang, Y., Chen, M.-L., 2020. Molybdenum isotopic behavior during intense weathering of basalt on Hainan Island, South China. Geochimica et Cosmochimica Acta.

Lu, X., Kendall, B., Stein, H.J., Li, C., Hannah, J.L., Gordon, G.W., Ebbestad, J.O.R., 2017. Marine redox conditions during deposition of Late Ordovician and Early Silurian organic-rich mudrocks in the Siljan ring district, central Sweden. Chemical Geology 457, 75-94.

Lutfi Firdaus, M., Norisuye, K., Nakagawa, Y., Nakatsuka, S., Sohrin, Y., 2008. Dissolved and labile particulate Zr, Hf, Nb, Ta, Mo and W in the western North Pacific Ocean. Journal of Oceanography 64, 247-257.

Madore, L., Caron, G., 2019. Mineral production in Québec in 2016, Mining by the numbers. Institut de la statistique du Québec, p. 16.

Malinovsky, D., Hammarlund, D., Ilyashuk, B., Martinsson, O., Gelting, J., 2007. Variations in the isotopic composition of molybdenum in freshwater lake systems. Chemical Geology 236, 181-198.

Malm, O., Pfeiffer, W.C., Souza, C.M., Reuther, R., 1990. Mercury pollution due to gold mining in the Madeira River basin, Brazil. ambio 19, 11-15.

Marks, J.A., Perakis, S.S., King, E.K., Pett-Ridge, J., 2015. Soil organic matter regulates molybdenum storage and mobility in forests. Biogeochemistry 125, 167-183.

Marx, S.K., Kamber, B.S., 2010. Trace-element systematics of sediments in the Murray–Darling Basin, Australia: Sediment provenance and palaeoclimate implications of fine scale chemical heterogeneity. Applied Geochemistry 25, 1221-1237.

McManus, J., Nägler, T.F., Siebert, C., Wheat, C.G., Hammond, D.E., 2002. Oceanic molybdenum isotope fractionation: Diagenesis and hydrothermal ridge-flank alteration. Geochemistry, Geophysics, Geosystems 3, 1-9.

McManus, J., Berelson, W.M., Severmann, S., Poulson, R.L., Hammond, D.E., Klinkhammer, G.P., Holm, C., 2006. Molybdenum and uranium geochemistry in continental margin sediments: Paleoproxy potential. Geochimica et Cosmochimica Acta 70, 4643-4662.

Morford, J.L., Emerson, S., 1999. The geochemistry of redox sensitive trace metals in sediments. Geochimica et Cosmochimica Acta 63, 1735-1750.

MERN, 2017 Liste des sites miniers abandonnés en date du 31 mars 2017, Energie et Resources naturellese Quebec. Retrieved from https://mern.gouv.qc.ca/mines/restauration-miniere/restauration-des-sites-miniers-abandonnes/ 17.05.2019

Millot, R., Gaillardet, J., Dupré, B., Allègre, C.J., 2002. The global control of silicate weathering rates and the coupling with physical erosion: new insights from rivers of the Canadian Shield. Earth and Planetary Science Letters 196, 83-98.

Miller, C.A., Peucker-Ehrenbrink, B., Walker, B.D., Marcantonio, F., 2011. Re-assessing the surface cycling of molybdenum and rhenium. Geochimica et Cosmochimica Acta 75, 7146-7179.

Nägler, T.F., Anbar, A.D., Archer, C., Goldberg, T., Gordon, G.W., Greber, N.D., Siebert, C., Sohrin, Y., Vance, D., 2014. Proposal for an International Molybdenum Isotope Measurement Standard and Data Representation. Geostandards and Geoanalytical Research 38, 149-151.

Nägler, T.F., Neubert, N., Böttcher, M.E., Dellwig, O., Schnetger, B., 2011. Molybdenum isotope fractionation in pelagic euxinia: Evidence from the modern Black and Baltic Seas. Chemical Geology 289, 1-11.

Nägler, T.F., Siebert, C., Lüschen, H., Böttcher, M.E., 2005. Sedimentary Mo isotope record across the Holocene fresh–brackish water transition of the Black Sea. Chemical Geology 219, 283-295.

Nägler, T., Pierret, M-C., Vögelin, A., Pettke, T., Aschwanden, L., and Villa, I.M., 2020. Small catchment scale Mo isotope balance and its implications for global Mo isotope cycling. In: Biogeochemical Cycles: Ecological Drivers and Environmental Impact. Geophysical Monograph Series: Vol. Book 248, 163-191. American Geophysical Union

Nakagawa, Y., Takano, S., Firdaus, M.L., Norisuye, K., Hirata, T., Vance, D., Sohrin, Y., 2012. The molybdenum isotopic composition of the modern ocean. Geochemical Journal 46, 131-141.

1029 Neely, R.A., Gislason, S.R., Ólafsson, M., McCoy-West, A.J., Pearce, C.R., Burton, K.W., 2018.
1030 Molybdenum isotope behaviour in groundwaters and terrestrial hydrothermal systems, Iceland.
1031 Earth and Planetary Science Letters 486, 108-118.

1032 Neubert, N., Heri, A.R., Voegelin, A.R., Nägler, T.F., Schlunegger, F., Villa, I.M., 2011. The
1033 molybdenum isotopic composition in river water: Constraints from small catchments. Earth and
1034 Planetary Science Letters 304, 180-190.

1035 Neubert, N., Nägler, T.F., Böttcher, M.E., 2008. Sulfidity controls molybdenum isotope fractionation
1036 into euxinic sediments: Evidence from the modern Black Sea. Geology 36, 775-778.

1037 Ottawa River Regulation Planning Board, 2011, Online database "Historical Water Level and
1038 Streamflow Summary" retrieved from http://www.ottawariver.ca/ottawa-river-carillon.php
1039 05.11.2019

1040 Pagnanelli, F., Moscardini, E., Giuliano, V., Toro, L., 2004. Sequential extraction of heavy metals in
1041 river sediments of an abandoned pyrite mining area: pollution detection and affinity series.
1042 Environmental Pollution 132, 189-201.

1043 Parent, M., Occhietti, S., 1988. Late Wisconsinan deglaciation and Champlain sea invasion in the St.
1044 Lawrence valley, Québec. Géographie physique et Quaternaire 42, 215-246.

1045 Pearce, C.R., Burton, K.W., von Strandmann, P.A.E.P., James, R.H., Gíslason, S.U.R., 2010.
1046 Molybdenum isotope behaviour accompanying weathering and riverine transport in a basaltic
1047 terrain. Earth and Planetary Science Letters 295, 104-114.

1048 Pearce, C.R., Cohen, A.S., Coe, A.L., Burton, K.W., 2008. Molybdenum isotope evidence for global
1049 ocean anoxia coupled with perturbations to the carbon cycle during the Early Jurassic. Geology 36,
1050 231-234.

1051 Percival, J.A., Skulski, T., Sanborn-Barrie, M., Stott, G.M., Leclair, A.D., Corkery, M.T., Boily, M.,
1052 2012. Geology and tectonic evolution of the Superior Province, Canada, Tectonic styles in Canada:
1053 the LITHOPROBE perspective. Geological Association of Canada St. Johns, NL, Canada, 321-378.

1054 Rahaman, W., Goswami, V., Singh, S.K., Rai, V.K., 2014. Molybdenum isotopes in two Indian
1055 estuaries: Mixing characteristics and input to oceans. Geochimica et Cosmochimica Acta 141, 407-
1056 422.

1057 Romaniello, S.J., Herrmann, A.D., Anbar, A.D., 2016. Syndepositional diagenetic control of
1058 molybdenum isotope variations in carbonate sediments from the Bahamas. Chemical Geology 438,
1059 84-90.

1060 Rondeau, B., Cossa, D., Gagnon, P., Pham, T.T., Surette, C., 2005. Hydrological and biogeochemical
1061 dynamics of the minor and trace elements in the St. Lawrence River. Applied Geochemistry 20,
1062 1391-1408.

1063 Rye, R. and Holland, H.D., 1998. Paleosols and the evolution of atmospheric oxygen: a critical
1064 review. American Journal of Science, 298(8), p.621.

1065 Sanford, B.V., Stott, D.F. and Aitken, J.D., 1993. St. Lawrence platform-geology. Sedimentary cover
1066 of the craton in Canada. Edited by DF Stott and JD Aitken. Geological Survey of Canada, Geology
1067 of Canada, 5, 723-786.

1068 Scott, C., Lyons, T.W., Bekker, A., Shen, Y., Poulton, S.W., Chu, X., Anbar, A.D., 2008. Tracing the
1069 stepwise oxygenation of the Proterozoic ocean. Nature 452, 456-459.

1070 Scott, C., Lyons, T.W., 2012. Contrasting molybdenum cycling and isotope properties in euxinic
1071 versus non-euxinic sediments and sedimentary rocks: Refining the paleoproxies. Chemical Geology
1072 324–325, 19-27.

1073 Seo, J.H., Guillong, M., Heinrich, C.A., 2012. Separation of Molybdenum and Copper in Porphyry
1074 Deposits: The Roles of Sulfur, Redox, and pH in Ore Mineral Deposition at Bingham Canyon.
1075 Economic Geology 107, 333-356.

1076 SIDEX 2007 Exploring for Molybdenum in Quebec, retrieved from
1077 http://www.sidex.ca/en/2015/02/16/exploring-for-molybdenum-in-quebec/ 17.04.2019

1078 Siebert, C., Nägler, T.F., Kramers, J.D., 2001. Determination of molybdenum isotope fractionation by
1079 double-spike multicollector inductively coupled plasma mass spectrometry. Geochemistry,
1080 Geophysics, Geosystems 2,(7)

1081 Siebert, C., Nägler, T.F., von Blanckenburg, F., Kramers, J.D., 2003. Molybdenum isotope records as
1082 a potential new proxy for paleoceanography. Earth and Planetary Science Letters 211, 159-171.

1083 Siebert, C., Pett-Ridge, J.C., Opfergelt, S., Guicharnaud, R.A., Halliday, A.N., Burton, K.W., 2015.
1084 Molybdenum isotope fractionation in soils: Influence of redox conditions, organic matter, and
1085 atmospheric inputs. Geochimica et Cosmochimica Acta 162, 1-24.

1086 Silva, L.F., de Vallejuelo, S.F.-O., Martinez-Arkarazo, I., Castro, K., Oliveira, M.L., Sampaio, C.H.,
1087 de Brum, I.A., de Leão, F.B., Taffarel, S.R., Madariaga, J.M., 2013. Study of environmental
1088 pollution and mineralogical characterization of sediment rivers from Brazilian coal mining acid
1089 drainage. Science of the total environment 447, 169-178.

1090 Skierszkan, E.K., Mayer, K.U., Weis, D., Beckie, R.D., 2016. Molybdenum and zinc stable isotope
1091 variation in mining waste rock drainage and waste rock at the Antamina mine, Peru. Science of The
1092 Total Environment 550, 103-113.

1093 Skierszkan, E.K., Robertson, J.M., Lindsay, M.B.J., Stockwell, J.S., Dockrey, J.W., Das, S., Weis, D.,
1094 Beckie, R.D., Mayer, K.U., 2019. Tracing Molybdenum Attenuation in Mining Environments Using
1095 Molybdenum Stable Isotopes. Environmental Science & Technology 53, 5678-5686.

1096 Skierszkan, E.K., Stockwell, J.S., Dockrey, J.W., Weis, D., Beckie, R.D., Mayer, K.U., 2017.
1097 Molybdenum (Mo) stable isotope variations as indicators of Mo attenuation in mine waste-rock
1098 drainage. Applied Geochemistry 87, 71-83.

1099 Slessarev, E.W., Lin, Y., Bingham, N.L., Johnson, J.E., Dai, Y., Schimel, J.P., Chadwick, O.A., 2016.
1100 Water balance creates a threshold in soil pH at the global scale. Nature 540, 567-569.

1101 Smolders, A., Lock, R., Van der Velde, G., Hoyos, R.M., Roelofs, J., 2003. Effects of mining
1102 activities on heavy metal concentrations in water, sediment, and macroinvertebrates in different
1103 reaches of the Pilcomayo River, South America. Archives of Environmental Contamination and
1104 Toxicology 44, 0314-0323.

1105 Solongo, T., Fukushi, K., Altansukh, O., Takahashi, Y., Akehi, A., Baasansuren, G., Ariuntungalag,
1106 Y., Enkhjin, O., Davaajargal, B., Davaadorj, D., 2018. Distribution and Chemical Speciation of
1107 Molybdenum in River and Pond Sediments Affected by Mining Activity in Erdenet City, Mongolia.
1108 Minerals 8, 288.

1109 Taylor, S.R., McLennan, S.M., 1985. The continental crust: Its composition and evolution. United
1110 States.

1111 Telmer, K., Veizer, J., 1999. Carbon fluxes, pCO_2 and substrate weathering in a large northern river
1112 basin, Canada: carbon isotope perspectives. Chemical Geology 159, 61-86.

1113 Thoby, M., Konhauser, K.O., Fralick, P.W., Altermann, W., Visscher, P.T., Lalonde, S.V., 2019.
1114 Global importance of oxic molybdenum sinks prior to 2.6 Ga revealed by the Mo isotope
1115 composition of Precambrian carbonates. Geology 47, 559-562.

1116 Thorp, J.H., Lamberti, G.A., Casper, A.F., 2005. 22 - St. Lawrence River Basin, in: Benke, A.C.,
1117 Cushing, C.E. (Eds.), Rivers of North America. Academic Press, Burlington, 982-1028.

1118 Torres, M.A., Baronas, J.J., Clark, K.E., Feakins, S.J., West, A.J., 2017. Mixing as a driver of
1119 temporal variations in river hydrochemistry: 1. Insights from conservative tracers in the Andes-
1120 Amazon transition. Water Resources Research 53, 3102-3119.

1121 Ventura, G.T., Gall, L., Siebert, C., Prytulak, J., Szatmari, P., Hürlimann, M., Halliday, A.N., 2015.
1122 The stable isotope composition of vanadium, nickel, and molybdenum in crude oils. Applied
1123 Geochemistry 59, 104-117.

1124 Voegelin, A.R., Nägler, T.F., Beukes, N.J., Lacassie, J.P., 2010. Molybdenum isotopes in late
1125 Archean carbonate rocks: Implications for early Earth oxygenation. Precambrian Research 182, 70-
1126 82.

1127 Voegelin, A.R., Nägler, T.F., Pettke, T., Neubert, N., Steinmann, M., Pourret, O., Villa, I.M., 2012.
1128 The impact of igneous bedrock weathering on the Mo isotopic composition of stream waters:
1129 Natural samples and laboratory experiments. Geochimica et Cosmochimica Acta 86, 150-165.

1130 Voegelin, A.R., Nägler, T.F., Samankassou, E., Villa, I.M., 2009. Molybdenum isotopic composition
1131 of modern and Carboniferous carbonates. Chemical Geology 265, 488-498.

1132 Wang, Z., Ma, J., Li, J., Wei, G., Chen, X., Deng, W., Xie, L., Lu, W., Zou, L., 2015. Chemical
1133 weathering controls on variations in the molybdenum isotopic composition of river water: Evidence
1134 from large rivers in China. Chemical Geology 410, 201-212.

1135 Wang, Z., Ma, J., Li, J., Wei, G., Zeng, T., Li, L., Zhang, L., Deng, W., Xie, L., Liu, Z., 2018. Fe
1136 (hydro) oxide controls Mo isotope fractionation during the weathering of granite. Geochimica et
1137 Cosmochimica Acta 226, 1-17.

1138 Wang, Z., Ma, J., Li, J., Zeng, T., Zhang, Z., He, X., Zhang, L., Wei, G., 2020. Effect of Fe–Ti oxides
1139 on Mo isotopic variations in lateritic weathering profiles of basalt. Geochimica et Cosmochimica
1140 Acta 286, 380-403.

1141 Weiss, D.J., Rehkdmper, M., Schoenberg, R., McLaughlin, M., Kirby, J., Campbell, P.G., Arnold, T.,
1142 Chapman, J., Peel, K., Gioia, Simone, 2008. Application of nontraditional stable-isotope systems to
1143 the study of sources and fate of metals in the environment. ACS Publications.

1144 Wen, H., Carignan, J., Zhang, Y., Fan, H., Cloquet, C., Liu, S., 2011. Molybdenum isotopic records
1145 across the Precambrian-Cambrian boundary. Geology 39, 775-778.

1146 Wheat, C.G., Mottl, M.J., Rudnicki, M., 2002. Trace element and REE composition of a low-
1147 temperature ridge-flank hydrothermal spring. Geochimica et Cosmochimica Acta 66, 3693-3705.

1148 Wieser, M.E., de Laeter, J.R., 2003. A preliminary study of isotope fractionation in molybdenites.
1149 International Journal of Mass Spectrometry 225, 177-183.

1150 Willbold, M., Hibbert, K., Lai, Y.J., Freymuth, H., Hin, R.C., Coath, C., Vils, F. and Elliott, T., 2016.
1151 High-precision mass-dependent Molybdenum isotope variations in magmatic rocks determined by
1152 double-spike MC-ICP-MS. Geostandards and Geoanalytical Research, 40(3), 389-403.

Wille, M., Kramers, J.D., Nägler, T.F., Beukes, N.J., Schröder, S., Meisel, T., Lacassie, J.P., Voegelin, A.R., 2007. Evidence for a gradual rise of oxygen between 2.6 and 2.5 Ga from Mo isotopes and Re-PGE signatures in shales. Geochimica et Cosmochimica Acta 71, 2417-2435.

Wille, M., Nägler, T.F., Lehmann, B., Schröder, S., Kramers, J.D., 2008. Hydrogen sulfide release to surface waters at the Precambrian/Cambrian boundary. Nature 453, 767-769.

Xu, L., Lehmann, B., Mao, J., Nägler, T.F., Neubert, N., Böttcher, M.E., Escher, P., 2012. Mo isotope and trace element patterns of Lower Cambrian black shales in South China: Multi-proxy constraints on the paleoenvironment. Chemical Geology 318, 45-59.

Yang, C., Telmer, K., Veizer, J., 1996. Chemical dynamics of the "St. Lawrence" riverine system: δD_{H_2O}, $\delta^{18}O_{H_2O}$, $\delta^{13}C_{DIC}$, $\delta^{34}S_{sulfate}$, and dissolved $^{87}Sr/^{86}Sr$. Geochimica et Cosmochimica Acta 60, 851-866.

Yeghicheyan D, Carignan J, Valladon M, Le Coz MB, Cornec FL, Castrec-Rouelle M, Robert M, Aquilina L, Aubry E, Churlaud C, Dia A, Deberdt S, Dupré B, Freydier R, Gruau G, Hénin O, de Kersabiec A-M, Macé J, Marin L, Morin N, Petitjean P, Serrat E (2001) A compilation of silicon and thirty one trace elements measured in the natural river water reference material SLRS-4 (NRC-CNRC). Geostand Newslett 25:465–474

Zeng, J., Han, G., Zhu, J.-M., 2019. Seasonal and Spatial Variation of Mo Isotope Compositions in Headwater Stream of Xijiang River Draining the Carbonate Terrain, Southwest China. Water 11, 1076.

Zhao, P.P., Li, J., Zhang, L., Wang, Z.B., Kong, D.X., Ma, J.L., Wei, G.J. and Xu, J.F., 2016. Molybdenum mass fractions and isotopic compositions of international geological reference materials. Geostandards and Geoanalytical Research, 40(2), 217-226.

Zhou, L., Algeo, T.J., Shen, J., Hu, Z., Gong, H., Xie, S., Huang, J., Gao, S., 2015. Changes in marine productivity and redox conditions during the Late Ordovician Hirnantian glaciation. Palaeogeography, Palaeoclimatology, Palaeoecology 420, 223-234.

Zhou, L., Su, J., Huang, J., Yan, J., Xie, X., Gao, S., Dai, M., Tonger, 2011. A new paleoenvironmental index for anoxic events—Mo isotopes in black shales from Upper Yangtze marine sediments. Science China Earth Sciences 54, 1024-1033.

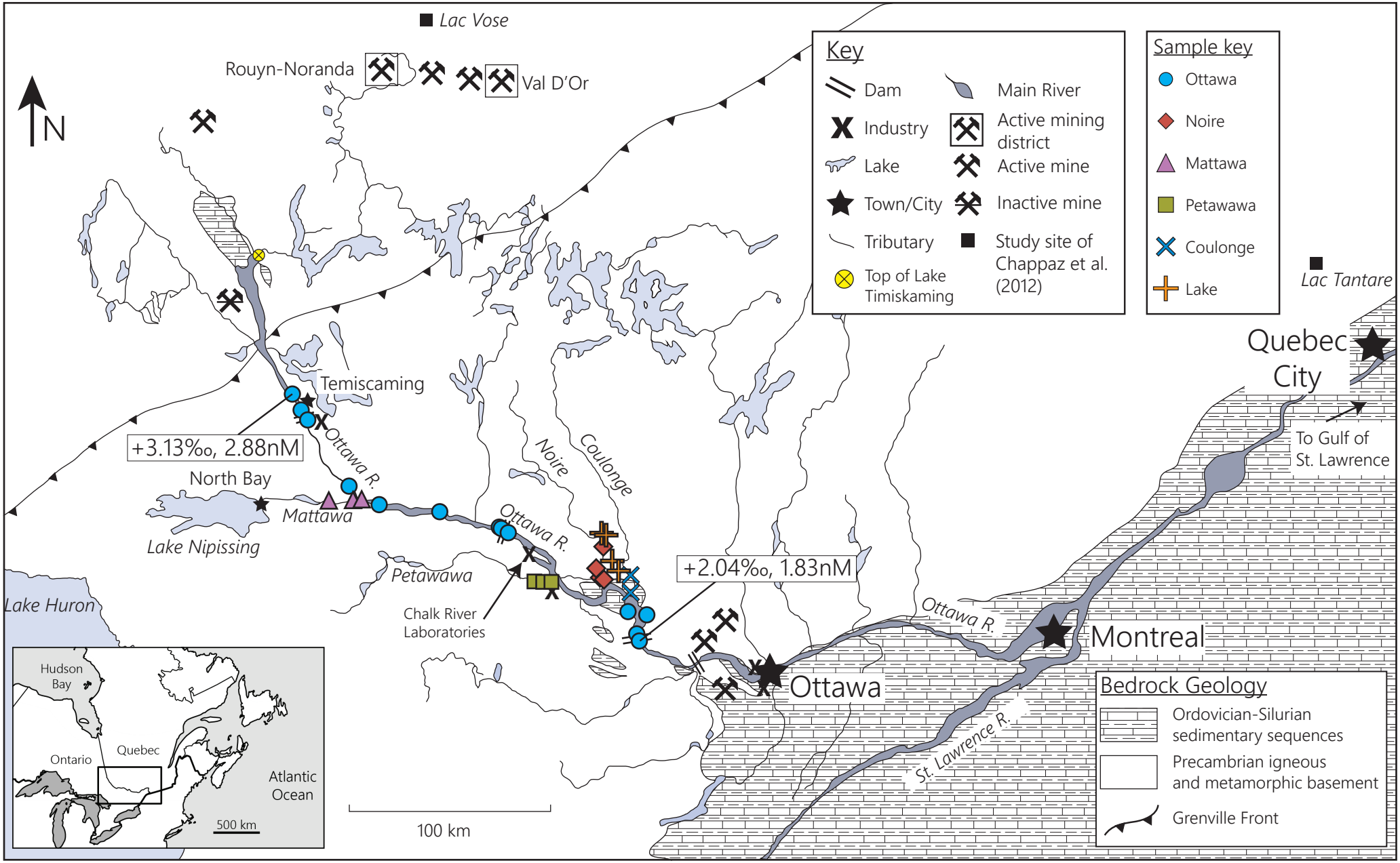
Lac Vose
Rouyn-Noranda
Val D'Or
N
Key
Dam
Main River
Industry
Active mining district
Lake
Active mine
Town/City
Inactive mine
Tributary
Study site of Chappaz et al. (2012)
Top of Lake Timiskaming
Sample key
Ottawa
Noire
Mattawa
Petawawa
Coulonge
Lake
Lac Tantare
Quebec City
To Gulf of St. Lawrence
Temiscaming
+3.13‰, 2.88nM
Ottawa R.
North Bay
Mattawa
Lake Nipissing
Noire
Coulonge
Ottawa R.
Petawawa
Chalk River Laboratories
+2.04‰, 1.83nM
Lake Huron
Ottawa R.
Montreal
Ottawa
St. Lawrence R.
Bedrock Geology
Ordovician-Silurian sedimentary sequences
Precambrian igneous and metamorphic basement
Grenville Front
Hudson Bay
Ontario
Quebec
Atlantic Ocean
500 km
100 km

Figure 2

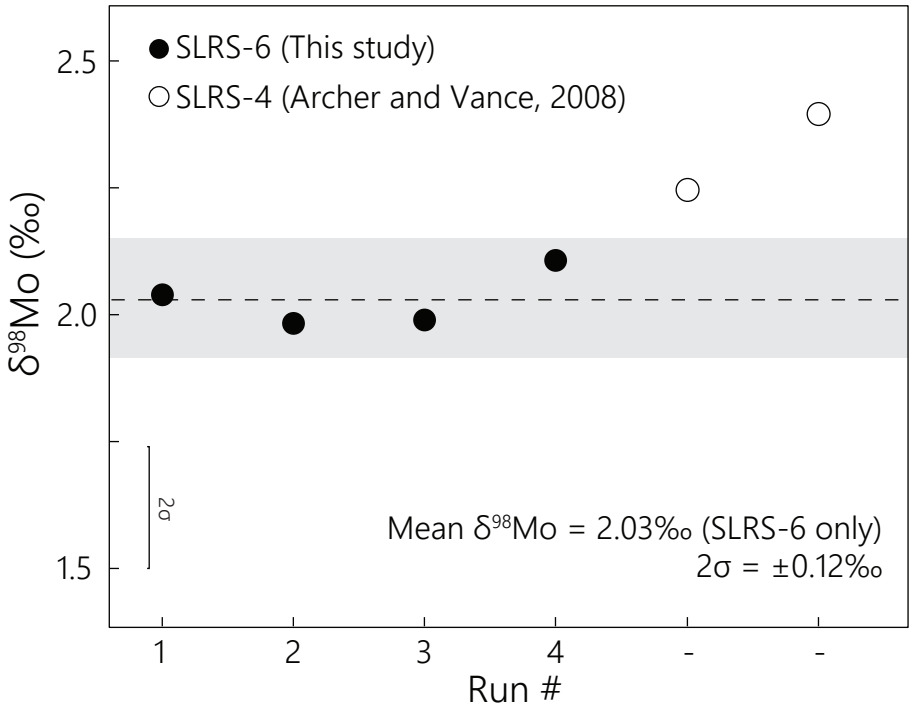
SLRS-6 (This study)
SLRS-4 (Archer and Vance, 2008)
2.5
2.0
1.5
δ98Mo (‰)
2σ
Mean δ98Mo = 2.03‰ (SLRS-6 only)
2σ = ±0.12‰
1
2
3
4
-
-
Run #

Figure 3

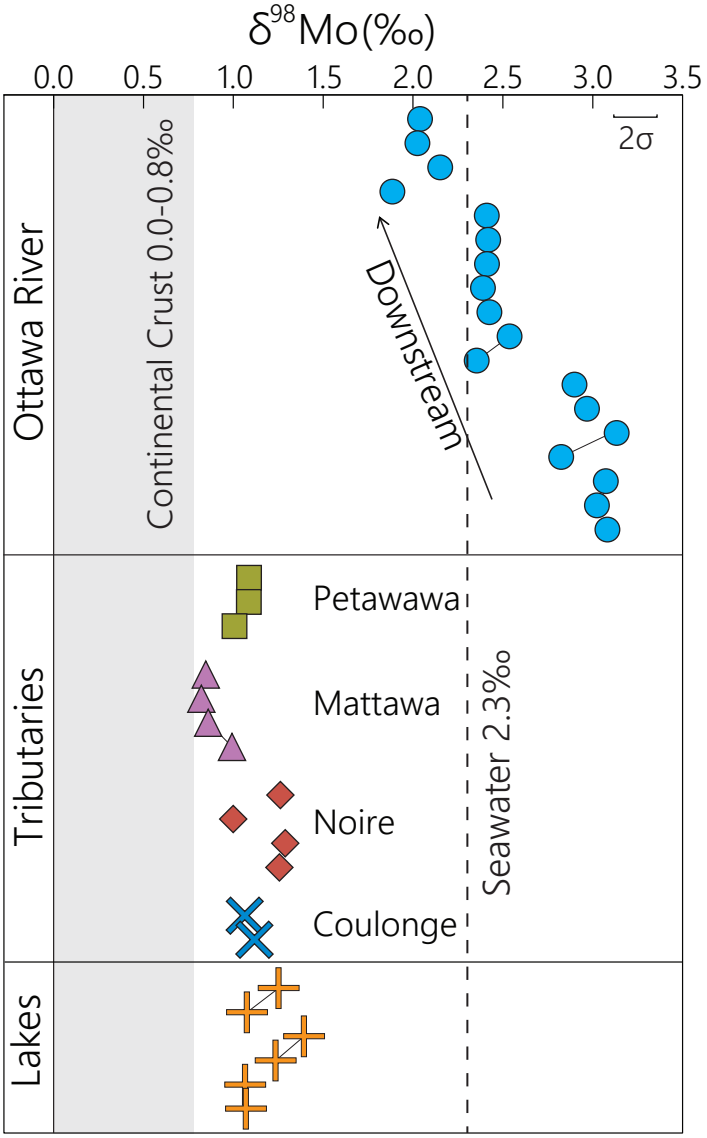
δ98Mo(‰)
0.0
0.5
1.0
1.5
2.0
2.5
3.0
3.5
Ottawa River
Tributaries
Lakes
Continental Crust 0.0-0.8‰
Seawater 2.3‰
2σ
Downstream
Petawawa
Mattawa
Noire
Coulonge

Figure 4

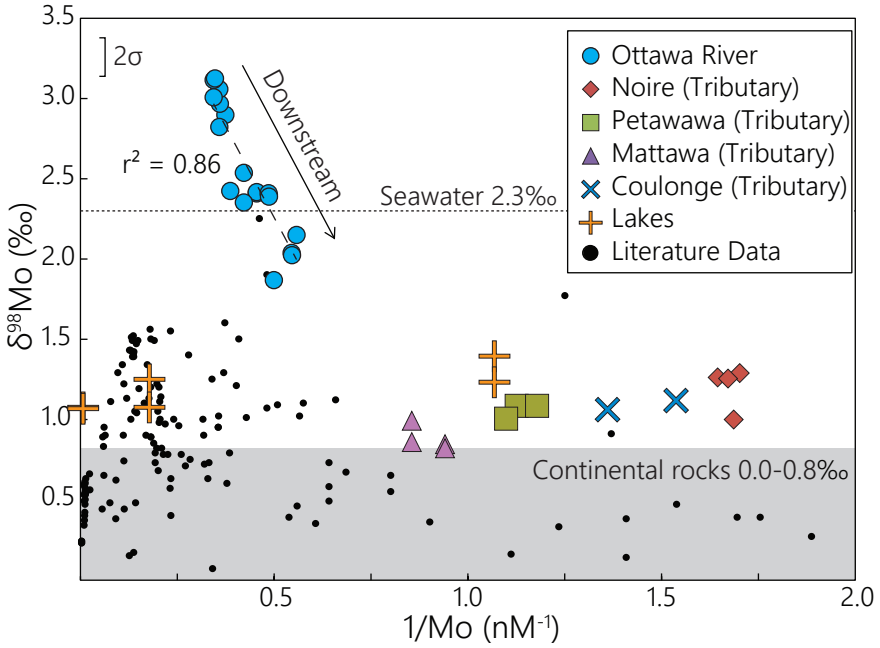
3.5
3.0
2.5
2.0
1.5
1.0
0.5
δ98Mo (‰)
2σ
r2 = 0.86
Downstream
Seawater 2.3‰
Continental rocks 0.0-0.8‰
Ottawa River
Noire (Tributary)
Petawawa (Tributary)
Mattawa (Tributary)
Coulonge (Tributary)
Lakes
Literature Data
0.5
1.0
1.5
2.0
1/Mo (nM-1)

Figure 5

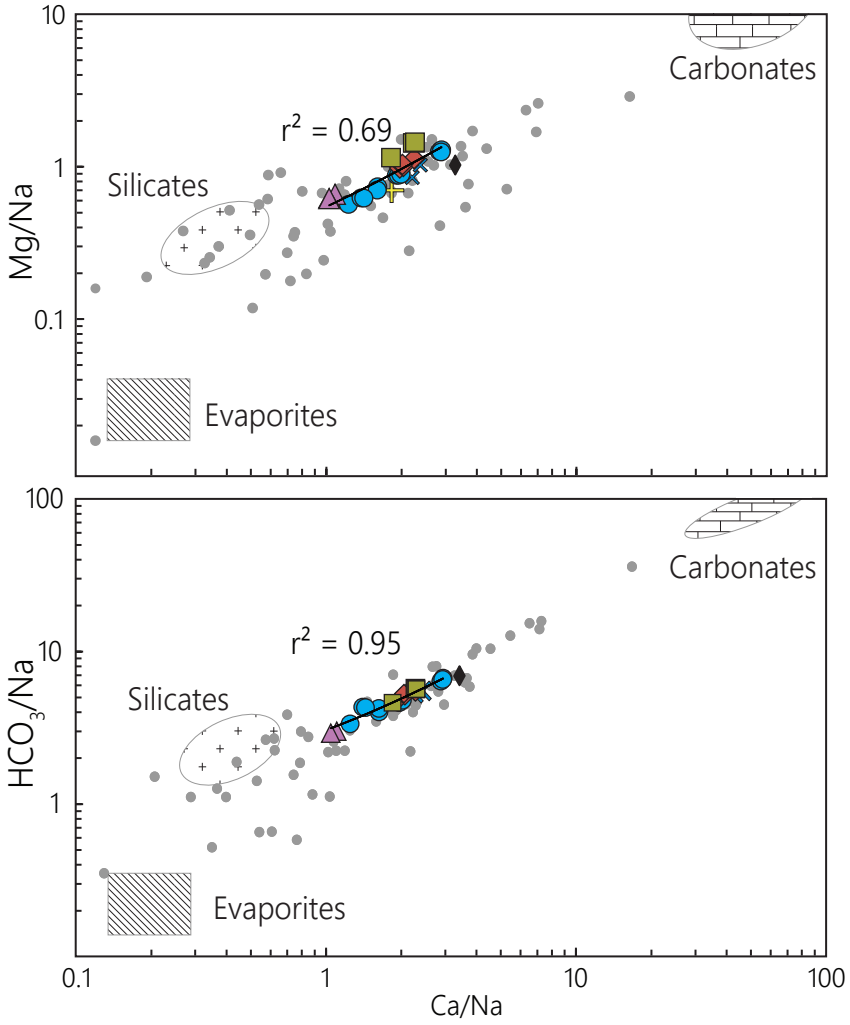
10
1
0.1
Mg/Na
Carbonates
r² = 0.69
Silicates
Evaporites
100
10
1
HCO3/Na
Carbonates
r² = 0.95
Silicates
Evaporites
0.1
1
10
100
Ca/Na

Figure 6

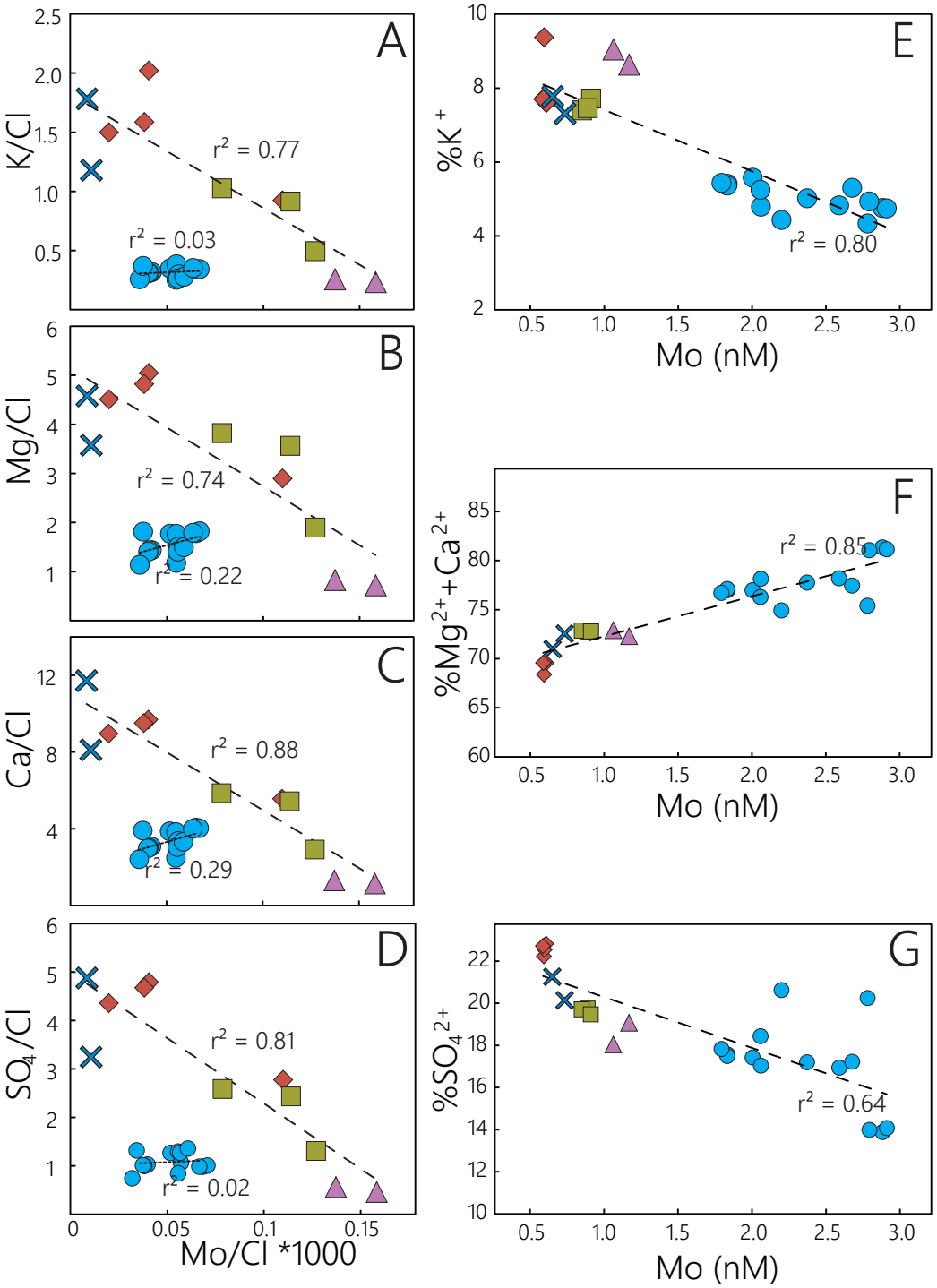
A
K/Cl
r² = 0.77
r² = 0.03
B
Mg/Cl
r² = 0.74
r² = 0.22
C
Ca/Cl
r² = 0.88
r² = 0.29
D
SO4/Cl
r² = 0.81
r² = 0.02
Mo/Cl *1000
E
%K+
r² = 0.80
Mo (nM)
F
%Mg2++Ca2+
r² = 0.85
Mo (nM)
G
%SO4 2+
r² = 0.64
Mo (nM)

Figure 7

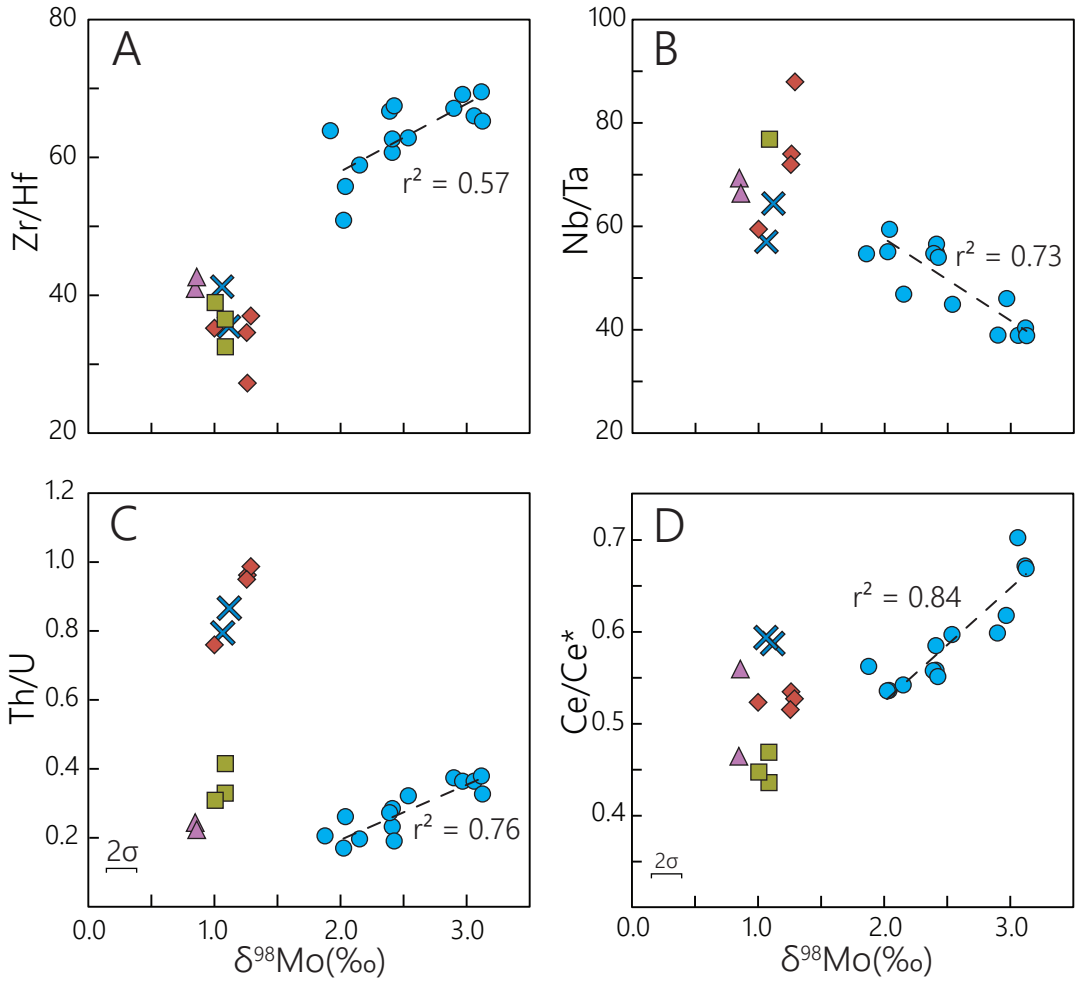
A
Zr/Hf
80
60
40
20
r² = 0.57
B
Nb/Ta
100
80
60
40
20
r² = 0.73
C
Th/U
1.2
1.0
0.8
0.6
0.4
0.2
2σ
r² = 0.76
0.0
1.0
2.0
3.0
δ⁹⁸Mo(‰)
D
Ce/Ce*
0.7
0.6
0.5
0.4
2σ
r² = 0.84
0.0
1.0
2.0
3.0
δ⁹⁸Mo(‰)

Figure 8

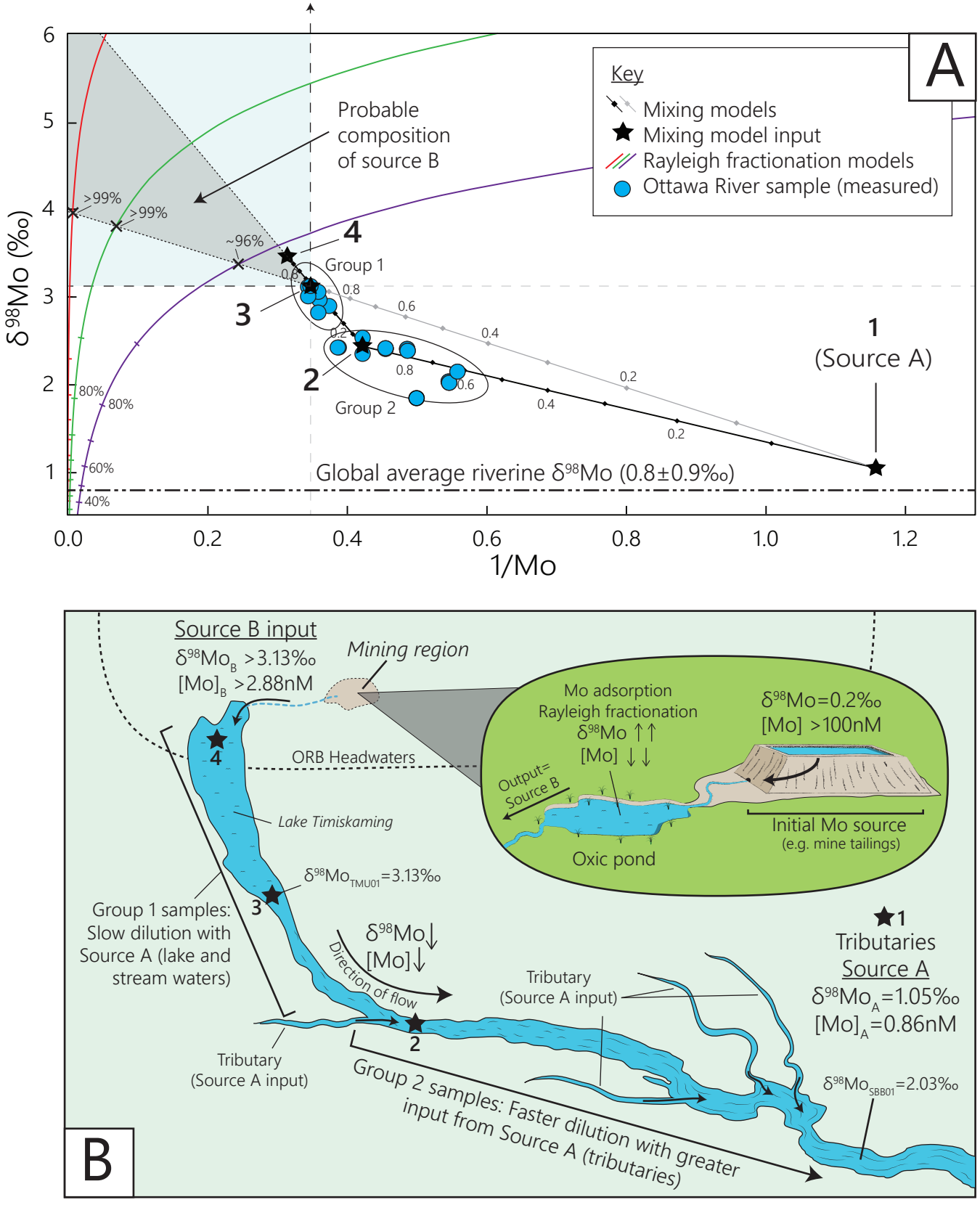
A
Key
Mixing models
Mixing model input
Rayleigh fractionation models
Ottawa River sample (measured)
Probable composition of source B
>99%
>99%
~96%
80%
80%
60%
40%
Group 1
Group 2
1 (Source A)
2
3
4
Global average riverine δ98Mo (0.8±0.9‰)
δ98Mo (‰)
1/Mo
B
Source B input
δ98MoB >3.13‰
[Mo]B >2.88nM
Mining region
Mo adsorption
Rayleigh fractionation
δ98Mo ↑↑
[Mo] ↓↓
δ98Mo=0.2‰
[Mo] >100nM
Output= Source B
Oxic pond
Initial Mo source
(e.g. mine tailings)
ORB Headwaters
Lake Timiskaming
δ98MoTMU01=3.13‰
Group 1 samples: Slow dilution with Source A (lake and stream waters)
δ98Mo↓
[Mo]↓
Direction of flow
★1
Tributaries
Source A
δ98MoA=1.05‰
[Mo]A=0.86nM
Tributary (Source A input)
Tributary (Source A input)
δ98MoSBB01=2.03‰
Group 2 samples: Faster dilution with greater input from Source A (tributaries)

Figure 1. Simplified hydrological map of the Ottawa River basin showing the Ottawa River, major tributaries and lakes, sampling locations and a selection of active and abandoned mines and mining districts, and industrial areas. Only tributaries sampled in this study are named (Noire, Coulonge, Mattawa, Petawawa). Black squares show locations of two lakes (Lac Vose and Lac Tantare) studied by Chappaz et al. (2012). Yellow circle with cross shows the uppermost traceable point of the Ottawa River, used in upstream extrapolation of δ^{98}Mo values (see section 5.5). Mo isotope values of uppermost and lowermost samples of the Ottawa River are shown for reference.

Figure 2. Plot of repeated measurements of reference material SLRS-6 (filled circles) and two measurements of SLRS-4 (open circles) as reported in Archer and Vance (2008). All data is normalised to reference material NIST 3134. Literature data is re-normalised for comparison with the current data. Dashed line indicates the average δ^{98}Mo of SLRS-6 of 2.03‰ as measured in this study. Grey shaded area represents 2σ reproducibility of ±0.11‰. Individual measurement $2\sigma_{\bar{x}}$ uncertainties are smaller than symbol size.

Figure 3. Variation in δ^{98}Mo between the Ottawa River, tributaries, and lakes. The data points for rivers are arranged from downstream (top) to upstream (bottom) to emphasize spatial variations. Dashed line represents the average seawater δ^{98}Mo composition (e.g., Nakagawa *et al.,* 2012). Grey shaded area indicates range of reported continental crust values (Greber *et al.,* 2014; Greber *et al.,* 2015; Horan *et al.,* 2020; Liu *et al.,* 2020; Pearce *et al.,* 2010; Siebert *et al.,* 2003; Voegelin *et al.,* 2014; Willbold *et al.,* 2016; Zhao *et al.,* 2016). Blue circles - Ottawa River; green squares - Petawawa River; purple triangles - Mattawa River; red diamonds - River Noire; blue crosses - Coulonge River; orange crosses - lakes. Symbols connected by black lines represent repeated measurements of the same sample (order in sequence for repeats does not represent order of analysis). 2σ external reproducibility is 0.11‰. $2\sigma_{\bar{x}}$ of individual measurements are smaller than symbols.

Figure 4. Plot of inverse Mo concentration and δ^{98}Mo data for 29 samples from the Ottawa River, tributaries and lakes (37 measurements including the 8 additional repeated measurements), and a compilation of other river water data as per King and Pett-Ridge (2018). The global average river water signature reported here is based on the weighted average of all literature data plotted (black circles). Dashed trend line and r^2 value refer to Ottawa River samples only. 2σ external reproducibility is ±0.11‰. $2\sigma_{\bar{x}}$ of individual measurements are smaller than symbols. Dashed line represents the average seawater δ^{98}Mo composition (e.g., Nakagawa *et al.,* 2012). Grey shaded area indicates range of continental crust values (e.g., Siebert *et al.,* 2003).

Figure 5. Plot of Na-normalised molar ratios of Mg and Ca (top) and HCO_3 and Ca (bottom) (after Gaillardet *et al.,* 1999) showing that the Ottawa River and its tributaries fall on a linear trend line between the composition expected for carbonate- and silicate-dominated river waters. For comparison is the composition of the Ottawa River at its mouth (Telmer and Veizer, 1999; yellow cross), an average compiled value of the St. Lawrence River (Gaillardet *et al.* 1999; black diamond), and other selected global river data (Gaillardet *et al.* 1999; grey circles). The r^2 values pertain to the Ottawa River + tributary data only. All sample data are corrected for marine aerosol input using Cl (see text for details). Silicate, carbonate and evaporite end member data from Gaillardet *et al.,* (1999). All other symbols outlined in Figure 3.

Figure 6. A-D: Plots comparing Mo content to selected major cations and anions indicative of weathering source. All elements are normalised to Cl^- to account for differing fluvial discharge (see text for details). Dashed line is a regression (with r^2 values) through the tributary data, whereas the dotted line is a regression (with r^2 values) through only the Ottawa River data. E-G: Mo content compared to contribution of major ions as a percentage of the sum of the four ions K^+, Mg^{2+}, Ca^{2+} and SO_4^{2-}. Dashed line is a regression (with r^2 value) through all Ottawa River + tributary data. Symbols are outlined in Figure 3.

Figure 7. Plots comparing δ^{98}Mo with selected molar HFSE ratios (Zr/Hf, Nb/Ta, Th/U) and the Ce anomaly (Ce/Ce*). All trace element data reported originally in Babechuk *et al.* (2020). Ce/Ce* calculated from upper crustal-normalized mass ratios using the geometric mean equations outlined in Lawrence *et al.* (2006) as per Babechuk *et al.* (2020). Dashed line is a regression (with r^2 value) through only the Ottawa River data. Symbols are outlined in Figure 3.

Figure 8. A: Interpreted model to explain the correlated downstream decrease in [Mo] and δ^{98}Mo in the Ottawa River (blue circles) that involves the progressive dilution of unknown Mo Source B (high [Mo] and δ^{98}Mo) with Mo Source A (low [Mo] and δ^{98}Mo). The Ottawa River samples are divided into two groups (Group 1 and Group 2) based on change in slope/trend interpreted to be related to a change in catchment tributary dilution. Black stars represent four points used to construct the downstream dilution model: 1) average tributary composition from this study (Source A); 2) furthest upstream sample of Group 2; 3) furthest upstream sample of Group 1 (furthest upstream measured in this study); 4) estimated composition of the furthest upstream point of the Ottawa River at top of Lake Timiskaming (see text). Dilution lines are calculated as binary mixtures between Source A and either Black Star 2 or Black Star 4, with fractions indicating the amount of Ottawa River water in the calculated mixture. The latter mixing lines are extended upstream to demonstrate the inferred composition of Source B assuming uniform mixing with Source A. The light grey shaded section indicates the entire range of possible compositions of Source B in terms of δ^{98}Mo and Mo concentration assuming the furthest upstream sample is a minimum composition. The darker grey shaded section indicates probable range of source B compositions constrained by the mixing models. Coloured lines indicate theoretical progression of mine drainage water δ^{98}Mo compositions assuming progressive Rayleigh fractionation upon adsorption to Fe-oxides (using fraction factor of 1.0010 from Skierszkan et al., 2019). Assumed initial mine drainage water composition taken as: Thompson Creek (3554nM, 0.6‰; Skierszkan *et al.,* 2019; red line); Clear Creek (508nM, 0.2‰; Archer and Vance, 2008; green line); Mo content 5 times lower than that of Clear Creek, with δ^{98}Mo equal to reported molybdenite ore from Don Rouyn (100nM, 0.2‰; Breillat *et al.,* 2016; purple line). Percentages indicate % removal of Mo from river or mine drainage water onto oxides generated by Rayleigh fractionation, with the minimum percent removal required to result in the δ^{98}Mo composition estimated for Source B. The stippled line at δ^{98}Mo of 0.8‰ is the global river water weighed average δ^{98}Mo calculated from the annual Mo discharge and Mo isotope compilation data of King and Pett-Ridge (2018). **B:** Graphic illustration of the dilution model in *A*. Bubble inset shows close-up of envisioned fractionation process within a mining region in the headwaters of the Ottawa River following the model described by Skierszkan et al. (2019; see text). Blue dashed line represents yet undefined flow path for Source B between mining region and Lake Timiskaming. Exact locations of mining regions and Source B input are not yet determined and are placed here for illustrative purposes. Black stars represent same points used in dilution models in *A*.

Table 1. Sample descriptions and locations

Sample ID	River	Location	Coordinates		Type
Ottawa River			**Latitude**	**Longitude**	
RRR01A	Ottawa	Foresters Falls	45°43'09.1''	76°43'17.1''	Open river above dam
PDF01A	Ottawa	Portage du Fort	45°35'33.6''	76°40'06.07''	Reservoir
SBB01A	Ottawa	Steamboat Bay	45°34’32.6”	76°40’13.5”	Below dam
CBM01A	Ottawa	Campbell's Bay	45°44'02.5''	76°36'14.5''	Open river above dam
RJR01A	Ottawa	Rolphton	46°11'17.1''	77°42'10.3''	Reservoir - centre of reservoir
RJR02A	Ottawa	Rolphton	46°11'20.1''	77°42'02.7''	Reservoir - lakeside
RJL01A	Ottawa	Rolphton	46°11'31.6''	77°41'02.8''	Below dam
KLR01A	Ottawa	Klock	46°17'30.9''	78°29'32.1''	Open river, open and narrow
BCR01A	Ottawa	Bissett Creek	46°13'35.6''	78°03'55.7''	Open river, in embayment
MAC01A	Ottawa	Mattawa Adventure Camp	46°19'15.4''	78°38'04.8''	Open river
OAR01B	Ottawa	Antoine Park	46°21'13.6''	78°43'37.5''	Open river below dam
TML01A	Ottawa	Temiscaming	46°42'00.42''	79°05'55.1''	River below industry/dam
TMU01A	Ottawa	Temiscaming	46°46'23.50"	79°08'02.7''	River above dam/industry
TMD01A	Ottawa	Temiscaming	46°42'39.95''	79°06'20.14''	Dam/reservoir west side branch, at paper mill
Tributaries					
BRU01A	Noire	Waltham	45°59'01.6''	76°50'08.9''	Open river above dam
BRR01A	Noire	Waltham	45°55'14.1''	76°55'11.6''	Reservoir - above dam
BRU02A	Noire	Waltham	45°56'27.6''	76°52'47.2''	Open river above dam
BRL01A	Noire	Waltham	45°54'45.40"	76°56'2.80"	Open river below dam
CRU01A	Coulonge	Fort Coulonge	45°54'38.3''	76°40'10.6''	Open river
CRL01A	Coulonge	Fort Coulonge	45°51'40.0''	76°44'29.3''	Open river
PWM01A	Petawawa	Outside Petawawa	45°53'11.7''	77°18'47.1''	Open river
PWL01A	Petawawa	Centennial Park	45°54'12.8''	77°16'45.6''	Open river/urban/quarry influence
PWU01A	Petawawa	Black Bay	45°52'54.4''	77°22'36.6''	River - slow flow, labelled as lake
MWL01A	Mattawa	Mattawa	46°18'57.4''	78°42'31.5''	Open river above estuary
MWU01A	Mattawa	Samuel de Champlain	46°18'01.09''	78°52'20.51''	Open river
Lakes					
CTL01A	Chemin Truite	-	45°56'05.4''	76°45'46.1''	Natural lake
PPL01A	Unnamed lake	Uphill from Lake Sauriol	45°58'34.4''	76°49'25.2''	Pond/precipitation catchment
CGL01A	Lac Vert	-	46°03'09.7''	76°52'00.3''	Natural lake
SLL01A	Lacs Sauriol	-	45°58'39.8''	76°49'11.0''	Natural lake

Table 2. Field parameter data

Sample ID	River	Temp[a] °C	Eh[b] mV	pH[c]	SpC µS/cm	DO mg/L
Ottawa Main						
RRR01A	Ottawa	24.8	-	7.6	51.2	3.5
PDF01A	Ottawa	26.2	-	7.6	54.2	7.0
SBB01A	Ottawa	24.7	-	7.4	50.8	4.6
CBM01A	Ottawa	24.3	-	7.5	52.1	4.3
RJR01A	Ottawa	27.7	212.5	8.1	64.3	8.3
RJR02A	Ottawa	28.2	202.0	8.3	57.4	15.5
RJL01A	Ottawa	19.7	262.5	7.3	50.8	14.2
Repeat		21.7	-	7.4	59.2	12.9
KLR01A	Ottawa	23.1	241.0	7.4	61.9	13.8
BCR01A	Ottawa	24.9	227.0	8.1	64.7	15.7
MAC01A	Ottawa	22.0	-	7.3	64.4	14.7
OAR01B	Ottawa	21.4	-	7.4	64.3	14.9
TML01A	Ottawa	22.0	-	7.5	57.5	15.0
TMU01A	Ottawa	23.9	-	7.4	59.6	14.8
TMD01A	Ottawa	24.0	-	7.6	59.9	14.6
Tributaries						
BRU01A	Noire	21.9	289.5	7.1	23.6	5.5
BRR01A	Noire	26.0	281.0	7.1	25.8	13.6
BRU02A	Noire	24.2	259.0	7.0	24.8	12.4
BRL01A	Noire	24.4	284.0	7.0	25.0	13.0
CRU01A	Coulonge	25.8	303.5	7.1	23.6	14.4
CRL01A	Coulonge	25.2	266.0	6.3	24.9	8.9
PWM01A	Petawawa	25.6	301.0	7.3	36.2	14.0
PWL01A	Petawawa	26.2	274.0	7.6	38.5	14.6
PWU01A	Petawawa	25.7	296.5	7.4	36.0	13.8
MWL01A	Mattawa	25.4	-	7.3	44.1	14.4
MWU01A	Mattawa	26.7	-	7.5	45.2	14.4
Lakes						
CTL01A	Chemin Truite	25.9	231.0	8.2	93.9	13.1
PPL01A	Unnamed lake	26.7	157.0	9.6	71.8	10.5
CGL01A	Lac Vert	27.8	177.0	9.1	81.8	10.6
SLL01A	Lake Sauriol	26.2	224.0	8.0	47.5	7.4

[a] Average of 4 measurements

[b] Average of two measurements with two separate instruments

[c] Instrument reading fluctuated max. ± 0.3

Table 3 Major ion and total organic carbon (TOC) data

Sample ID	River	Na^+ µM	K^+ µM	Ca^{2+} µM	Mg^{2+} µM	Cl^- µM	SO_4^{2-} µM	HCO_3^- mM	TOC mg/L
Ottawa Main									
SBB01A	Ottawa	89.30	14.63	129.2	56.07	43.64	45.83	0.38	7.05
PDF01A	Ottawa	88.04	14.96	132.4	58.82	44.96	46.27	0.39	7.07
RRR01A	Ottawa	89.00	14.65	133.7	56.60	44.65	46.40	0.39	6.66
CBM01A	Ottawa	101.7	14.53	129.9	56.85	56.08	46.04	0.39	6.85
RJL01A	Ottawa	95.69	15.12	147.7	64.29	39.61	49.30	0.50	7.95
RJR01A	Ottawa	90.87	14.50	137.4	60.18	36.84	47.52	0.47	7.21
RJR02A	Ottawa	92.35	15.32	138.0	59.69	37.57	47.65	0.52	7.43
BCR01A	Ottawa	125.1	15.93	163.5	70.71	50.24	54.26	0.41	7.58
KLR01A	Ottawa	150.2	17.37	151.9	68.00	63.16	56.80	0.42	7.97
MAC01A	Ottawa	151.2	17.26	171.6	74.04	48.86	60.85	0.43	8.17
OAR01B	Ottawa	149.5	16.85	176.0	75.07	47.33	62.23	0.53	8.43
TML01A	Ottawa	78.69	15.65	173.8	75.61	44.01	44.73	0.48	7.85
TMD01A	Ottawa	89.21	16.09	170.1	74.00	43.53	45.04	0.49	7.58
TMU01A	Ottawa	81.73	17.26	170.8	74.33	44.34	45.13	0.49	7.97
Tributaries									
PWL01A	Petawawa	50.98	15.58	79.35	48.33	29.65	39.63	0.20	5.65
PWM01A	Petawawa	56.94	14.91	77.58	46.94	15.68	39.01	0.20	5.84
PWU01A	Petawawa	63.85	15.78	78.43	46.73	14.64	38.68	0.21	5.65
MWL01A	Mattawa	102.6	19.26	80.32	46.61	76.87	36.50	0.20	6.19
MWU01A	Mattawa	105.3	18.36	82.82	48.58	68.94	39.82	0.20	5.61
BRL01A	Noire	41.80	14.73	57.61	25.46	11.59	32.79	0.18	5.76
BRR01A	Noire	41.11	11.53	57.88	25.26	6.714	32.52	0.29	5.90
BRU01A	Noire	46.50	11.59	59.33	25.67	6.996	33.09	0.29	7.46
BRU02A	Noire	39.89	11.76	58.98	25.50	7.447	32.85	0.28	6.48
CRL01A	Coulonge	38.10	10.46	62.24	23.49	8.519	28.10	0.29	8.10
CRU01A	Coulonge	35.80	10.08	56.61	22.09	5.529	27.26	0.29	7.54
Lakes									
CTL01A	Lake	50.28	15.83	333.1	75.65	21.58	50.39	0.40	4.45
SLL01A	Lake	29.80	11.23	154.9	32.29	11.76	39.11	0.72	6.92
PPL01A	Lake	31.06	11.13	226.9	41.51	9.760	63.13	0.85	10.2
CGL01A	Lake	28.71	13.73	298.5	42.20	8.434	38.50	0.51	4.26

Table 4. Mo concentration, Mo isotope and selected trace element data

Sample ID	δ^{98}Mo	2 $\sigma_{\bar{x}}$	Mo[a]	Mo[b]	Sr[b]	Zr[b]	Nb[b]	Hf[b]	Ta[b]	W[b]	Th[b]	U[b]	Ce/Ce*[b,c]
	‰		nM	nM	µM	nM	pM	pM	pM	pM	pM	pM	
SLRS-6[d]	2.03	0.11[e]	2.06										
Ottawa River													
SBB01A	2.039	0.015	2.074	1.835	0.3034	358	24.9	6.42	0.418	49.56	57.2	219	0.545
PDF01A	2.024	0.012	2.277	1.832	0.3001	272	19.6	5.35	0.356	50.58	37.0	217	0.545
RRR01A	2.151	0.013	2.225	1.793	0.2843	338	20.9	5.73	0.446	54.11	39.6	201	0.552
CBM01A	1.849	0.017	2.395	2.004	0.3167	366	24.9	5.72	0.454	67.26	55.9	272	0.572
RJL01A	2.410	0.012	2.446	2.199	0.2663	642	40.4	10.6	0.735	90.73	59.4	255	0.595
(Repeat)	2.418	0.019	2.961										
RJR01A	2.411	0.013	2.564	2.060	0.2595	562	30.3	8.96	0.536	89.83	70.1	246	0.568
RJR02A	2.389	0.014	2.601	2.057	0.2606	520	27.4	7.79	0.500	86.92	66.3	243	0.567
BCR01A	2.425	0.017	2.537	2.589	0.2883	608	27.2	9.01	0.503	89.52	55.5	290	0.561
KLR01A	2.537	0.035	2.668	2.372	0.3016	812	49.6	12.9	1.10	63.93	88.0	273	0.607
(Repeat)	2.354	0.013	2.432										
MAC01A	2.899	0.014	2.575	2.677	0.2478	1110	37.7	16.6	0.967	73.06	107	286	0.609
OAR01B	2.968	0.019	2.850	2.781	0.2531	1200	54.7	17.3	1.19	74.61	106	291	0.629
TML01A	3.178	0.014	2.889	2.793	0.2905	1040	88.3	15.8	2.27	67.48	117	320	0.715
(Repeat)	2.824	0.013	3.306										
TMD01A	3.117	0.013	2.750	2.911	0.2851	958	63.0	13.8	1.56	67.26	123	323	0.683
(Repeat)	3.063	0.013	3.058										
TMU01A	3.126	0.014	2.882	2.882	0.2880	902	61.5	13.8	1.58	64.12	106	322	0.680

[a] This study

[b] Trace element and Ce/Ce* data from Babechuk *et al.* (2020), converted to molar concentrations

[c] Calculated according to geometric equations of Lawrence et al. (2006)

[d] Average of 4 measurements

[e] 2σ external reproducibility, n=4

Table 4. Continued

Sample ID	River	δ^{98}Mo ‰	2 $\sigma_{\bar{x}}$	Mo nM	Mo[b] nM	Sr[b] µM	Zr[b] nM	Nb[b] pM	Hf[b] pM	Ta[b] pM	W[a] pM	Th[b] pM	U[b] pM	Ce/Ce*[b]
Tributaries														
PWL01A	Petawawa	1.087	0.013	0.914	0.8883	0.3230	62.7	8.57	1.93	0.055	6.221	33.4	80.3	0.443
PWM01A	Petawawa	1.086	0.013	0.946	0.8489	0.3223	62.7	9.22	1.72	0.120	4.134	27.0	81.9	0.477
PWU01A	Petawawa	1.006	0.015	0.834	0.9104	0.3212	70.8	9.45	1.82	0.024	4.552	26.3	85.0	0.455
MWL01A	Mattawa	0.8475	0.017	1.026	1.063	0.3010	96.7	13.6	2.36	0.196	7.714	22.9	93.4	0.473
(Repeat)		0.8221	0.016	1.018										
MWU01A	Mattawa	0.8603	0.016	1.157	1.169	0.3037	92.4	16.8	2.17	0.253	11.26	20.4	91.0	0.569
(Repeat)		0.9934	0.016	1.376										
BRL01A	Noire	1.262	0.018	0.588	0.6081	0.2625	74.8	14.8	2.74	0.201	5.189	77.4	80.4	0.544
BRR01A	Noire	1.000	0.019	0.624	0.5932	0.2635	77.0	10.5	2.19	0.176	5.256	60.8	80.0	0.532
BRU01A	Noire	1.291	0.017	0.511	0.5877	0.2659	109	15.4	2.94	0.176	5.939	86.0	87.1	0.524
BRU02A	Noire	1.256	0.016	0.580	0.5983	0.2669	98.9	15.0	2.86	0.209	5.151	83.2	87.6	0.536
CRL01A	Coulonge	1.064	0.016	0.822	0.7345	0.3006	140	23.0	3.38	0.403	8.787	83.2	105	0.604
CRU01A	Coulonge	1.118	0.013	0.767	0.6506	0.2829	126	21.9	3.55	0.340	5.398	84.2	97.0	0.060
Lakes														
CTL01A	Lake	1.350	0.014	5.748	5.610	0.7330	12.7	b.d.l.	b.d.l.	b.d.l.	14.6	1.96	104	-
(Repeat)		1.120	0.017	6.252										
SLL01A	Lake	1.395	0.016	0.871	0.9360	0.5502	18.0	b.d.l.	b.d.l.	b.d.l.	6.66	7.81	39.3	-
(Repeat)		1.235	0.018	1.103										
PPL01A	Lake	1.066	0.012	1.347	1.256	1.168	32.0	b.d.l.	b.d.l.	b.d.l.	12.7	7.94	92.9	-
CGL01A	Lake	1.071	0.018	2.320	1.736	0.8841	6.2	b.d.l.	b.d.l.	b.d.l.	10.5	1.73	180	-

[a] This study

[b] Trace element and Ce/Ce* data from Babechuk *et al.* (2020), converted to molar concentrations

[c] Calculated according to geometric equations of Lawrence et al. (2006)

[d] Average of 4 measurements

[e] 2σ external reproducibility, n=4

Unusually heavy stable Mo isotope signatures of the Ottawa River: causes and implications for global riverine Mo fluxes

O'Sullivan, E.M., Nägler, T.F. and Babechuk, M.G.

Supplementary information, tables and figures

1. Binary mixing model calculations (Section 5.4; Figure 8)

The samples of groups 1 and 2 of the Ottawa River samples fall on two of three mixing lines constructed among four points within the ORB: 1) average tributary composition from this study (Source A); 2) furthest upstream sample of Group 2; 3) furthest upstream sample of Group 1 (furthest upstream measured in this study); 4) estimated composition of the furthest upstream point of the Ottawa River at top of Lake Timiskaming (see below). In the following calculations, each of these points are assumed to represent theoretical "end members" where F=1. Note that these models do not depict a binary mixing between two true end members *per se*, but the progressive downstream dilution of Source B by Source A.

1. Binary mixing models

The inverse Mo concentration 1/[Mo] of a series of theoretical mixtures (*mix*) at different points along the mixing line where F=0.1 to 0.9 is calculated as

$$1/[Mo]_{mix} = 1/([Mo]_i F_i + (1 - F_i)[Mo]_j)$$

where *F* denotes the fraction of each "end member" in the mixture, and *i* and *j* represent the two chosen points out of 1-4 above. The isotope composition (δ) is then defined for each of these intermediate points as

$$\delta_{mix} = \frac{[Mo]_i F_i \delta_i + (1 - F_i)[Mo]_j \delta_j}{[Mo]_{mix}}$$

Solving the equation of the line where x=0 allows the estimation of a theoretical point where the line crosses the y axis at 1/[Mo]=0, to extrapolate the composition of Ottawa River water upstream of these known points.

2. Estimation of composition of point 4 (furthest upstream point of the Ottawa River at top of Lake Timiskaming)

The average rate of change in δ^{98}Mo and [Mo] in group 1 was used to estimate the composition of the Ottawa River water at the top of Lake Timiskaming. Approximate distances between samples along the river measured using Google Earth and changes in Mo concentration and isotope composition with distance are as follows:

Sample	Distance from previous sample	Cumulative distance	[Mo]	δ^{98}Mo	Δ [Mo]	Δ δ^{98}Mo
	km	km	nM	‰	nM/km	‰/km
TMU01	**0**	**0**	**2.88**	**3.13**	**0.003984**	**-0.00125**
TMD01	7.28	7.28	2.91	3.12	-0.08801	-0.04297
TML01	1.34	8.62	2.79	3.06	-0.00024	-0.00178
OAR01	51.3	59.92	2.78	2.97	-0.01066	-0.00712
MAC01	**9.73**	**69.65**	**2.68**	**2.90**	**-0.02656**	**-0.03151**

As the change in Mo concentration and isotope composition between each individual sample is somewhat irregular, the difference between the uppermost and lowermost samples (TMU01 and MAC01, respectively) were used to calculate an overall change in [Mo] of -0.21 nM and δ^{98}Mo of -0.23‰ over a distance of 69.65 km, resulting in a rate of change of 0.003 nM/km and 0.003‰/km for group 1 samples. The distance between the uppermost sample TMU01 and the top of Lake Timiskaming (Figure 1) measured on Google Earth is approximately 100 km. We predict an overall change of 0.30 nM Mo and 0.33‰ over that distance, resulting in an estimated [Mo] and δ^{98}Mo composition of point 4 of 3.18 nM and 3.45‰, respectively.

2. Supplementary Tables

Table S1. Mo isotope composition of samples repeated from bottles A (acidified within 2 weeks) and B (acidified after 6 months)

Sample ID	MWL01		MWU01		SLL01	
Bottle	A	B	A	B	A	B
Mo (nM)	1.026	1.018	1.157	1.376	0.871	1.103
δ^{98}Mo (‰)	0.847	0.822	0.860	0.993	1.395	1.235
$2\sigma_{\bar{x}}$	0.015	0.016	0.016	0.017	0.015	0.024
$\Delta_{A\text{-}B}$	0.025		0.133		0.159	

Table S2. Unit conversion of major cations from µM to meq/L

Sample ID	River	Na^+		K^+		Ca^{2+}		Mg^{2+}	
		µM	meq/L	µM	meq/L	µM	meq/L	µM	meq/L
Ottawa Main									
SBB01A	Ottawa	89.3	0.0824	14.6	0.0142	129	0.272	56.1	0.126
PDF01A	Ottawa	88.0	0.0831	15.0	0.0142	132	0.275	58.8	0.129
RRR01A	Ottawa	89.0	0.0826	14.7	0.0142	134	0.270	56.6	0.126
CBM01A	Ottawa	102	0.0975	14.5	0.0148	130	0.275	56.8	0.129
RJL01A	Ottawa	95.7	0.0900	15.1	0.0141	148	0.310	64.3	0.141
RJR01A	Ottawa	90.9	0.0866	14.5	0.0139	137	0.292	60.2	0.134
RJR02A	Ottawa	92.3	0.0869	15.3	0.0147	138	0.291	59.7	0.134
BCR01A	Ottawa	125	0.118	15.9	0.0153	164	0.342	70.7	0.152
KLR01A	Ottawa	150	0.141	17.4	0.0162	152	0.318	68.0	0.149
MAC01A	Ottawa	151	0.121	17.3	0.0132	172	0.301	74.0	0.139
OAR01B	Ottawa	150	0.124	16.9	0.0134	176	0.319	75.1	0.143
TML01A	Ottawa	78.7	0.0749	15.7	0.0153	174	0.361	75.6	0.157
TMD01A	Ottawa	89.2	0.0735	16.1	0.0152	170	0.354	74.0	0.159
TMU01A	Ottawa	81.7	0.0752	17.3	0.0159	171	0.358	74.3	0.160
Tributaries									
PWL01A	Petawawa	51.0	0.0609	15.6	0.0149	79.4	0.177	48.3	0.113
PWM01A	Petawawa	56.9	0.0513	14.9	0.0146	77.6	0.174	46.9	0.112
PWU01A	Petawawa	63.9	0.0510	15.8	0.0153	78.4	0.174	46.7	0.112
MWL01A	Mattawa	103	0.100	19.3	0.0182	80.3	0.181	46.6	0.112
MWU01A	Mattawa	105	0.0967	18.4	0.0179	82.8	0.185	48.6	0.115
BRL01A	Noire	41.8	0.0388	14.7	0.0109	57.6	0.131	25.5	0.0676
BRR01A	Noire	41.1	0.0379	11.5	0.0137	57.9	0.131	25.3	0.0680
BRU01A	Noire	46.5	0.0397	11.6	0.0112	59.3	0.134	25.7	0.0677
BRU02A	Noire	39.9	0.0392	11.8	0.0113	59.0	0.135	25.5	0.0675
CRL01A	Coulonge	38.1	0.0364	10.5	0.0102	62.2	0.140	23.5	0.0612
CRU01A	Coulonge	35.8	0.0339	10.1	0.0100	56.6	0.131	22.1	0.0508
Lakes									
CTL01A	Lake	50.3	0.0410	15.8	0.0132	333	0.628	75.6	0.144
SLL01A	Lake	29.8	0.0292	11.2	0.0110	155	0.335	32.3	0.0787
PPL01A	Lake	31.1	0.0301	11.1	0.0111	227	0.470	41.5	0.0980
CGL01A	Lake	28.7	0.0280	13.7	0.0133	299	0.637	42.2	0.0982

Table S3. Comparison of isobaric interference-correction of δ^{98}Mo values using 99/95 or 101/95 mass ratios

Sample	99/101	99/95	Corrected?[a]	101/95	Corrected?[a]	δ^{98}Mo*						
						Mass 99	2SE	Mass 101	2SE	Uncorrected	2SE	
						‰		‰		‰		
Ottawa												
SBB01	0.709	0.0010	Yes	0.0013	Yes	2.199	0.014	2.192	0.014	2.039	0.015	
PDF01	0.709	0.0009	Yes	0.0013	Yes	2.211	0.011	2.205	0.011	2.024	0.012	
RRR01	0.713	0.0009	Yes	0.0013	Yes	2.324	0.011	2.317	0.011	2.151	0.013	Downstream Chalk River
CBM01	0.687	0.0010	Yes	0.0014	Yes	2.349	0.017	2.048	0.017	1.849	0.029	
RJL01	0.708	0.0009	Yes	0.0013	Yes	2.603	0.011	2.596	0.011	2.410	0.012	Upstream Chalk River
(Repeat)	0.676	0.0001	No	0.0001	Yes	2.418	0.019	2.446	0.015	2.418	0.019	
RJR01	0.704	0.0010	Yes	0.0014	Yes	2.572	0.013	2.566	0.013	2.411	0.013	
RJR02	0.710	0.0009	Yes	0.0013	Yes	2.565	0.013	2.558	0.013	2.389	0.014	
BCR01	0.849	0.0016	Yes	0.0022	Yes	2.700	0.016	2.685	0.057	2.425	0.017	
KLR01	0.681	0.0010	Yes	0.0015	Yes	2.736	0.018	2.728	0.016	2.537	0.035	
(Repeat)	0.723	0.0014	Yes	0.0020	Yes	2.623	0.011	2.609	0.011	2.354	0.013	
MAC01	0.730	0.0007	Yes	0.0009	Yes	3.026	0.013	3.019	0.013	2.899	0.014	
OAR01	0.726	0.0008	Yes	0.0011	Yes	3.117	0.018	3.108	0.018	2.968	0.019	
TML01	0.735	0.0007	Yes	0.0009	Yes	3.185	0.013	3.178	0.013	3.059	0.014	
(Repeat)	0.734	0.0010	Yes	0.0013	Yes	2.960	0.012	2.948	0.012	2.824	0.013	
TMD01	0.736	0.0007	Yes	0.0009	Yes	3.229	0.012	3.221	0.012	3.117	0.013	Downstream Temiscaming
(Repeat)	0.889	0.0001	Yes	0.0001	Yes	3.063	0.021	3.059	0.021	3.008	0.013	
TMU01	0.727	0.0007	Yes	0.0009	Yes	3.254	0.013	3.246	0.013	3.126	0.014	Upstream Temiscaming

[a] Corrected if 99/95 or 101/95 >0.0001

*Corrected for isobaric interferences

Table S3. Continued

Sample	Δ98Mo*$_{99\text{-}101}$	Δ98Mo*$_{99\text{-}Uncorr}$	Δ98Mo*$_{101\text{-}Uncorr}$	
	‰	‰	‰	
Ottawa				
SBB01	0.007	0.161	0.154	
PDF01	0.006	0.187	0.180	
RRR01	0.007	0.173	0.166	Downstream Chalk River
CBM01	0.302	0.500	0.198	
RJL01	0.006	0.193	0.187	Upstream Chalk River
(Repeat)	-0.028	-	0.028	
RJR01	0.006	0.161	0.155	
RJR02	0.007	0.176	0.169	
BCR01	0.015	0.275	0.260	
KLR01	0.008	0.199	0.191	
(Repeat)	0.014	0.269	0.255	
MAC01	0.008	0.128	0.120	
OAR01	0.008	0.149	0.140	
TML01	0.007	0.126	0.119	
(Repeat)	0.011	0.136	0.124	
TMD01	0.008	0.112	0.104	Downstream Temiscaming
(Repeat)	0.004	0.054	0.050	
TMU01	0.007	0.128	0.121	Upstream Temiscaming

[a] Corrected if 99/95 or 101/95 >0.0001

*Corrected for isobaric interferences

Table S3. Continued

Sample	99/101	99/95	Corrected?[a]	101/95	Corrected?[a]	δ^{98}Mo*					
						Mass 99	2SE	Mass 101	2SE	Uncorrected	2SE
						‰		‰		‰	
Tributaries											
BRL01	0.743	0.0001	No	0.0001	No	1.262	0.018	1.262	0.018	1.262	0.018
BRR01	0.717	0.0015	Yes	0.0021	Yes	1.242	0.019	1.229	0.019	1.000	0.019
BRU01	0.726	0.0001	No	0.0001	Yes	1.290	0.017	1.302	0.017	1.290	0.017
BRU02	0.727	0.0001	No	0.0001	No	1.256	0.016	1.256	0.016	1.256	0.016
PWL01	0.668	0.0015	Yes	0.0021	Yes	1.349	0.013	1.334	0.025	1.087	0.013
PWM01	0.696	0.0015	Yes	0.0021	Yes	1.356	0.012	1.342	0.048	1.086	0.013
PWU01	0.721	0.0017	Yes	0.0024	Yes	1.304	0.012	1.288	0.013	1.006	0.015
MWL01	0.669	0.0016	Yes	0.0022	Yes	1.105	0.016	1.091	0.089	0.847	0.017
(Repeat)	0.764	0.0001	No	0.0001	No	0.822	0.016	0.822	0.016	0.822	0.016
MWU01	0.696	0.0016	Yes	0.0021	Yes	1.111	0.015	1.087	0.031	0.860	0.016
(Repeat)	0.593	0.0001	No	0.0001	Yes	0.993	0.016	1.005	0.017	0.993	0.016
CRL01	0.760	0.0001	No	0.0001	No	1.064	0.016	1.064	0.016	1.064	0.016
CRU01	0.698	0.0001	No	0.0001	No	1.118	0.013	1.118	0.012	1.118	0.013
Lakes											
CGL01	0.717	0.0010	Yes	0.0014	Yes	1.237	0.016	1.229	0.016	1.071	0.018
CTL01	0.738	0.0007	Yes	0.0010	Yes	1.359	0.013	1.350	0.013	1.252	0.014
(Repeat)	0.914	0.0002	Yes	0.0003	Yes	1.120	0.038	1.110	0.037	1.077	0.017
PPL01	0.710	0.0010	Yes	0.0013	Yes	1.223	0.012	1.216	0.012	1.066	0.012
SLL01	0.734	0.0001	No	0.0001	No	1.395	0.016	1.395	0.016	1.395	0.016
(Repeat)	0.799	0.0001	No	0.0001	Yes	1.235	0.018	1.522	0.023	1.235	0.018

[a]Correction applied if 99/95 or 101/95 >0.0001

*Corrected for isobaric interferences

Table S3. Continued

Sample	$\Delta 98Mo^*_{99\text{-}101}$	$\Delta 98Mo^*_{99\text{-}Uncorr}$	$\Delta 98Mo^*_{101\text{-}Uncorr}$
	‰	‰	‰
Tributaries			
BRL01	-	-	-
BRR01	0.013	0.241	0.229
BRU01	-0.013	-	0.013
BRU02	-	-	-
PWL01	0.015	0.262	0.247
PWM01	0.014	0.270	0.256
PWU01	0.016	0.298	0.282
MWL01	0.014	0.257	0.243
(Repeat)	-	-	-
MWU01	0.024	0.251	0.227
(Repeat)	-0.012	-	0.012
CRL01	-	-	-
CRU01	-	-	-
Lakes			
CGL01	0.009	0.167	0.158
CTL01	0.009	0.106	0.098
(Repeat)	0.010	0.043	0.033
PPL01	0.007	0.157	0.150
SLL01	-	-	-
(Repeat)	-0.286	-	0.286

[a]Correction applied if 99/95 or 101/95 >0.0001

*Corrected for isobaric interferences

Table S4. Mo concentration and δ^{98}Mo Results of repeated measurements of SLRS-6

Run #	δ^{98}Mo ‰	2 $\sigma_{\bar{x}}$	Mo nM
1	2.040	0.014	2.370
2	1.986	0.012	2.000
3	1.993	0.018	1.988
4	2.109	0.024	1.894
Average	2.03	0.11	2.06

[a] 2σ standard deviation

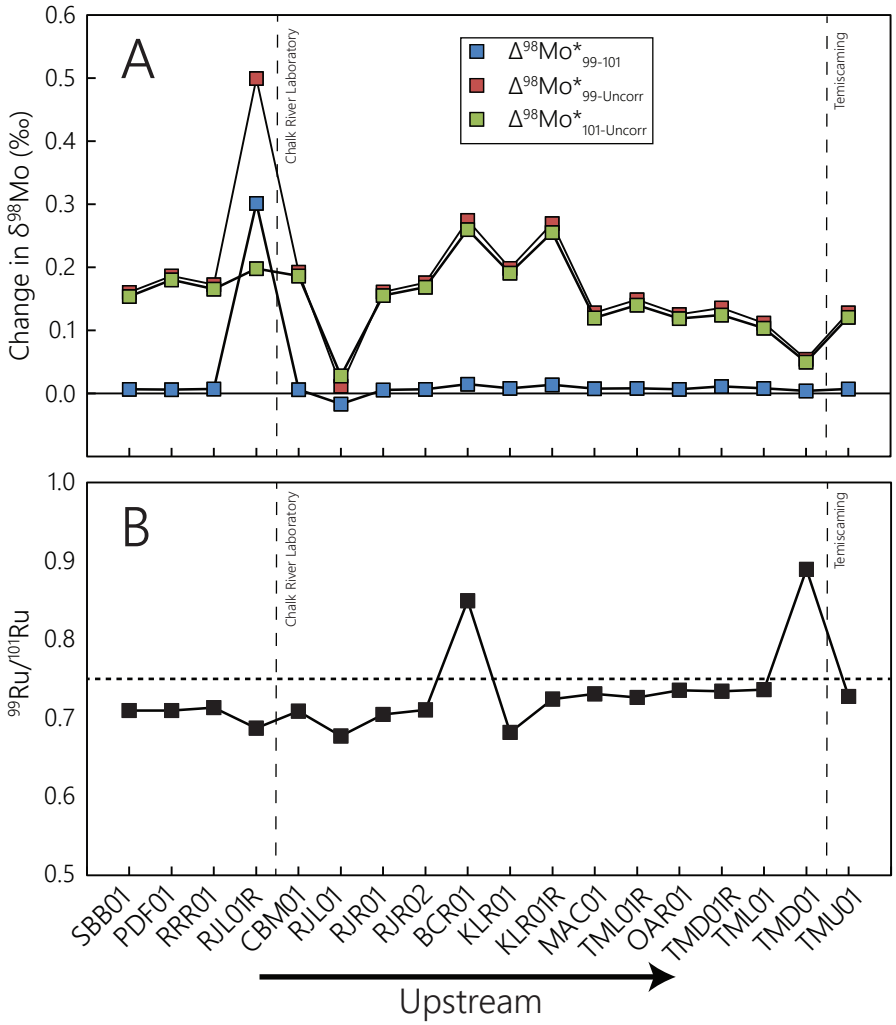

Figure S1. Plots comparing the effect of using mass ratios 99/95 and 101/95 as a correction for isobaric interferences of ^{99}Ru and ^{101}Ru on ^{98}Mo and ^{100}Mo of Ottawa River samples. A: Difference in calculated δ98Mo values of samples when corrected via mass 99 or 101 (subscripts 99- Uncorr, 101-Uncorr) compared to values without correction (subscript Uncorr) and differnce between both corrections (subscript 99-100). B: Measured 99/101 ratio of samples compared to the natural ratio (0.75, indicated by horizontal dotted line). Vertical dashed lines indicate relative location of Chalk River Laboratory and the pulp and paper factory at Temiscaming in terms of sample positioning/order along the river. Sample locations progress upstream from left to right.